

Article

Exploring New Physics with Deep Underground Neutrino Experiment High-Energy Flux: The Case of Lorentz Invariance Violation, Large Extra Dimensions and Long-Range Forces

Alessio Giarnetti , Simone Marciano  and Davide Meloni 

Dipartimento di Matematica e Fisica, Università di Roma Tre, INFN Sezione di Roma Tre,
Via della Vasca Navale 84, 00146 Roma, Italy; simone.marciano@uniroma3.it (S.M.);
davide.meloni@uniroma3.it (D.M.)

* Correspondence: alessio.giarnetti@uniroma3.it

Abstract: DUNE is a next-generation long-baseline neutrino oscillation experiment. It is expected to measure, with unprecedented precision, the atmospheric oscillation parameters, including the CP-violating phase δ_{CP} . Moreover, several studies have suggested that its unique features should allow DUNE to probe several new physics scenarios. In this work, we explore the performances of the DUNE far detector in constraining new physics if a high-energy neutrino flux is employed (HE-DUNE). We take into account three different scenarios: Lorentz Invariance Violation (LIV), Long-Range Forces (LRFs) and Large Extra Dimensions (LEDs). Our results show that HE-DUNE should be able to set bounds competitive to the current ones and, in particular, it can outperform the standard DUNE capabilities in constraining CPT-even LIV parameters and the compactification radius R_{ED} of the LED model.

Keywords: neutrino mixing; DUNE; BSM



Citation: Giarnetti, A.; Marciano, S.; Meloni, D. Exploring New Physics with Deep Underground Neutrino Experiment High-Energy Flux: The Case of Lorentz Invariance Violation, Large Extra Dimensions and Long-Range Forces. *Universe* **2024**, *10*, 357. <https://doi.org/10.3390/universe10090357>

Academic Editor: Roman Pasechnik

Received: 29 July 2024

Revised: 23 August 2024

Accepted: 28 August 2024

Published: 5 September 2024



Copyright: © 2024 by the authors. Licensee MDPI, Basel, Switzerland. This article is an open access article distributed under the terms and conditions of the Creative Commons Attribution (CC BY) license (<https://creativecommons.org/licenses/by/4.0/>).

1. Introduction

Neutrino oscillation discovery [1] represented a milestone in the history of particle physics. Indeed, the observation of this phenomenon unveiled that neutrinos have (tiny) masses compared to the other fermions of the Standard Model (SM) of particle physics. In addition, the small uncertainties achieved in the measurements of mixing angles carry us into a precision era in the neutrino sector, thanks to an effort that lasted 25 years and that has involved different particle sources: the Sun [2], the Earth atmosphere [3], nuclear reactors [4] and accelerator facilities [5]. The oscillation parameters involved in solar oscillation, namely the solar mixing angle θ_{12} and the solar mass splitting Δm_{21}^2 , have been precisely measured by several solar neutrino experiments and by a peculiar reactor experiment: KamLAND [6–8]. The reactor mixing angle θ_{13} , instead, was discovered and measured with an astonishing precision in 2012 [9], leaving the atmospheric oscillation sector less constrained. Indeed, the mixing angle θ_{23} is almost maximal ($\theta_{23} \in [40^\circ, 50^\circ]$ [10]) and suffers from the so-called *octant degeneracy*, which makes the determination of the octant in which θ_{23} lies (Higher Octant, HO, $\theta_{23} > 45^\circ$ or Lower Octant, LO, $\theta_{23} < 45^\circ$) very difficult to be determined. Moreover, according to the current neutrino oscillation data, the atmospheric mass splitting Δm_{31}^2 has an absolute value 30 times larger than the solar one and can still assume both positive and negative values. This is the so-called *mass hierarchy problem*.

The solution to these long-lasting problems might be given by the next generation of long-baseline (LBL) accelerator experiments. Such experiments are mainly sensitive to the atmospheric neutrino frequency and employ a well-known, focused, artificial muon neutrino flux coming from an accelerator facility. The two experiments that are expected to start their data-taking in the current decade are T2HK in Japan [11] and DUNE [12] in

the USA. The importance of such experiments lies not only in the solution of the octant and hierarchy problems but also in their unprecedented capabilities to measure the CP-violating phase δ_{CP} , for which T2K and NO ν A [13–15] have provided a first (weak) signal. Even though both experiments will be sensitive to the same neutrino oscillation regime, DUNE will have the advantage of running with a broad-band beam, allowing observation of neutrinos whose energy extends beyond the first oscillation maximum. To go even higher in energy, the possibility of using a high-energy (HE) neutrino beam in DUNE has been widely discussed. This would allow, for instance, collection of the largest ν_τ event sample ever observed [16]. In recent years, a large number of studies have shown that the employment of this particular flux might be extremely useful in exploring tiny new physics effects in neutrino oscillation in the presence, for instance, of sterile neutrinos, non-unitarity of the PMNS matrix, Non-Standard Interactions or quantum decoherence [16–21]. In this context, the advantage of using the HE flux lies in the fact that some models predicts new effects enhanced by neutrino energy. The extremely large collectable sample of events in all neutrino flavors provides a unique tool to study these energy-enhanced new physics effects.

In this paper, we explore and discuss the DUNE capabilities in its HE configuration to measure the new physics parameters involved in neutrino oscillation in three particular models: the Lorentz Invariance Violation (LIV), the Long-Range Forces (LRFs) and the Large Extra Dimensions (LEDs) models. In the first two cases, the Lagrangian interaction is supplemented with additional operators whose coefficients must be bounded from above, while in the last case, the space-time framework is enlarged by at least one spatial dimension (experienced by right-handed neutrinos only) whose radius belongs to the sub-millimeter range. Even though such new physics models have been investigated by other authors in the literature, our results show that the bounds that HE-DUNE can set on the model parameters are comparable with the existing ones and, for the CPT-even LIV parameters and for the radius of the LED model, can outperform the capabilities of the standard DUNE setup.

The paper will be organized as follows: in Section 2, we will describe the DUNE experiment and its HE configuration; in Sections 3–5, we discuss the LIV, LRF and LED models, respectively. Finally, in Section 6, we draw our conclusions.

2. The DUNE Experiment and the High-Energy Flux

The DUNE (Deep Underground Neutrino Experiment) experiment is a proposed long-baseline experiment in the USA [12,22–24]. The near detector complex, composed of different multi-purpose near detectors [25] as well as the accelerator facilities, is being built at Fermilab; on the other hand, the 40kt LAr-TPC detector will be located in South Dakota, roughly 1300 km away from the neutrino beam source. The on-axis neutrino beams will be mainly composed of ν_μ or $\bar{\nu}_\mu$ depending on the current circulating in the focusing horns; this will allow the experiment to run in both *neutrino* and *antineutrino* modes. The main purpose of the experiment is to precisely measure the oscillation parameters in the atmospheric sector. In particular, DUNE is expected to reach a great sensitivity to the mass hierarchy and an unprecedented sensitivity to the θ_{23} octant. Moreover, the experiment is also designed to maximize the sensitivity to the PMNS matrix phase δ_{CP} . In order to perform such a measurement, the proposed neutrino flux is a broad-band beam that peaks at around 2.5 GeV so sit at the first atmospheric oscillation maximum. This should allow observation of not only a huge sample of ν_μ events ($\mathcal{O}(10^3)$ per year) but also several ν_e appearance events ($\mathcal{O}(10^2)$ per year) [12,22–24]. A very intense flux of ν_τ will also arrive at the far detector; however, given the Charged Current (CC) ν_τ interaction energy threshold (3.1 GeV), only a minor fraction of these events might be observed. To overcome this problem and observe a larger number of τ neutrinos, a broader, high-energetic flux peaked at around 5 GeV has also been considered by the DUNE collaboration [26–28]. The main disadvantage of using this flux is that the performances in measuring standard oscillation parameters are poorer [16]. However, other than collecting the largest ν_τ sample ever obtained ($\mathcal{O}(10^2)$ in a year [16]), as already mentioned, the employment of such a flux has

been demonstrated to be very promising in constraining new physics scenarios [16–19]. Thus, a high-energy flux run, at least in addition to the standard DUNE one [18], might be extremely useful to provide unique information in the context of neutrino oscillation. In this work, we focus on the capabilities of the DUNE experiment to probe some beyond-the-Standard Model (BSM) theories that make an imprint on the neutrino oscillation probabilities, taking full advantage of the high-energy flux. From now on, we will refer to this DUNE configuration as HE-DUNE. In order to make a comparison with the standard DUNE results, for the HE-DUNE, we will use the same efficiencies, energy resolutions and systematic uncertainties provided by the collaboration for the standard DUNE [29,30]. In order to include the possible effects of the ν_τ appearance in constraining the new physics parameters space, we follow [16,18]. In particular, we make the hypothesis that the HE-DUNE might be able to observe 30% of the ν_τ events with subsequent $\tau \rightarrow e$ decays and 30% of the ν_τ events with subsequent hadronic τ decays. The systematic uncertainty for this channel has been set to a conservative 25% normalization error¹. Misidentified ν_μ , ν_e and NC events have been considered as a background to the ν_τ channel, according to [16,18].

The total running time for HE-DUNE has been fixed to 5 years in neutrino mode and 5 years in antineutrino mode. Finally, the whole analysis has been carried out neglecting the events observed at the near detectors and considering the final 40kt far detector for all the 10 years of data taking.

3. The Lorentz Invariance Violation Case

The Lorentz invariance is one of the fundamental symmetries of the SM and it is related to the space-time structure. The other essential symmetry of the quantum field theory is the CPT symmetry². Since the SM fails to unify all the forces governing the Universe, it has been taken into account the possibility that the SM is an effective theory of a wider framework that unifies not only electromagnetic and weak interactions, but also strong interactions and gravity. The energy scale of such a general theory should be the Planck mass ($M_P \sim 10^{19}$ GeV). In these SM extensions, CPT and Lorentz symmetries might be violated [31–40]; in particular, it has been shown that CPT breaking always leads to Lorentz Invariance Violation (LIV) as well [34]. Neutrino experiments could be able to probe LIV through suitable modification of the oscillation probabilities induced by the presence of new terms in the full theory. In the next subsection, we will show how the neutrino probabilities can be affected by LIV.

3.1. Theoretical Framework

In the presence of LIV, the neutrino Lagrangian density term can be written as [38,41,42]

$$\mathcal{L} = \frac{1}{2} \bar{\psi} (i \not{\partial} - M + Q) \psi + h.c., \tag{1}$$

where ψ is the neutrino fermionic field and the effect of the LIV is encoded in the generic operator Q . If we restrict ourselves to renormalizable Dirac couplings, the Lorentz Invariance violating Lagrangian terms can be written as [42,43]:

$$\mathcal{L}^{\text{LIV}} = -\frac{1}{2} \left(a_{\alpha\beta}^\mu \bar{\psi}_\alpha \gamma_\mu \psi_\beta + b_{\alpha\beta}^\mu \bar{\psi}_\alpha \gamma_5 \gamma_\mu \psi_\beta - ic_{\alpha\beta}^{\mu\nu} \bar{\psi}_\alpha \gamma_\mu \partial_\nu \psi_\beta - id_{\alpha\beta}^{\mu\nu} \bar{\psi}_\alpha \gamma_5 \gamma_\mu \partial_\nu \psi_\beta \right) + h.c.. \tag{2}$$

The first two terms are CPT-odd, while the third and the fourth terms are CPT-even. Thus, the LIV effect in the interaction Hamiltonian can be encoded in two Hermitian matrices:

$$\tilde{a}_{\alpha\beta}^\mu = (a + b)_{\alpha\beta}^\mu \quad \text{and} \quad \tilde{c}_{\alpha\beta}^{\mu\nu} = (c + d)_{\alpha\beta}^{\mu\nu}. \tag{3}$$

These matrices modify the standard neutrino oscillation Hamiltonian by adding a new term H_{LIV} to the vacuum and matter contributions:

$$H_\nu = H_m + H_\text{ae} + H_{\text{LIV}}, \tag{4}$$

where, as usual,

$$H_m = \frac{1}{2E} U \begin{pmatrix} 0 & 0 & 0 \\ 0 & \Delta m_{21}^2 & 0 \\ 0 & 0 & \Delta m_{31}^2 \end{pmatrix} U^\dagger \quad \text{and} \quad H_\alpha = \sqrt{2} G_F N_e \text{diag}(1, 0, 0). \quad (5)$$

Here, E is the neutrino energy, $\Delta m_{ij}^2 = m_i^2 - m_j^2$ are the neutrino mass splittings, U is the neutrino mixing matrix, which depends on three mixing angles (θ_{12} , θ_{13} and θ_{23}) and one complex phase δ_{CP} , G_F is the Fermi constant and N_e is the number density of electrons in the medium traversed by neutrinos. The term H_α corresponds to the well-known Mikheev–Smirnov–Wolfenstein (MSW) mechanism [44].

The last term H_{LIV} is the one induced by the LIV. On a general ground, it reads $H_{LIV} = 1/E(\tilde{a}^\mu p_\mu - \tilde{c}^{\mu\nu} p_\mu p_\nu)$, where p_μ is the neutrino four-momentum. However, focusing only on time-like LIV matrix components ($\mu, \nu = 0$) and considering a Sun-centered isotropic inertial frame (see [43] for details), the Lorentz Invariance Violation effects are governed by the parameters $\tilde{a}_{\alpha\beta}^0 \equiv a_{\alpha\beta}$ and $\tilde{c}_{\alpha\beta}^{00} \equiv c_{\alpha\beta}$. Being elements of Hermitian matrices, diagonal $(a, c)_{\alpha\alpha}$ are real, while off-diagonal $(a, c)_{\alpha\beta}$ are complex parameters uniquely determined by their moduli, which we denote as $(a, c)_{\alpha\beta}$, and their phases $\Phi_{\alpha\beta}$. Thus, the LIV Hamiltonian reads:

$$H_{LIV} = \begin{pmatrix} a_{ee} & a_{e\mu} & a_{e\tau} \\ a_{e\mu}^* & a_{\mu\mu} & a_{\mu\tau} \\ a_{e\tau}^* & a_{\mu\tau}^* & a_{\tau\tau} \end{pmatrix} - \frac{4}{3} E \begin{pmatrix} c_{ee} & c_{e\mu} & c_{e\tau} \\ c_{e\mu}^* & c_{\mu\mu} & c_{\mu\tau} \\ c_{e\tau}^* & c_{\mu\tau}^* & c_{\tau\tau} \end{pmatrix} \quad (6)$$

where, as already mentioned, $a_{\alpha\beta}$ ($c_{\alpha\beta}$) are CPT-odd (CPT-even) LIV parameters. Notice that the factor $-4/3$ comes from the fact that the trace of \tilde{c} is not observable and its diagonal space components must be related to its 00 component [43]. It is worth to mention that $a_{\alpha\beta}$ matrix has a similar structure to the propagation Non Standard Interaction (NSI) matrix. Even though there exists a direct correspondence between NSI and LIV parameters, it is important to notice that the two models affect neutrino oscillation in a different way: while NSIs necessitate neutrinos to travel through a matter medium, LIV modifies the oscillation probabilities also in vacuum [41,42,45,46].

Another important aspect of LIV effects is that the CPT-even ones are amplified by neutrino energy. For this reason, we expect a high-energy flux for the DUNE experiment to be more efficient in constraining them. From now on, we will only focus on the off-diagonal LIV parameters since they affect the most oscillations of neutrinos in a long-baseline experiment, as we will discuss below.

In order to have a feeling of the effect of the LIV on the oscillation parameters, we can write the correction to the $\nu_\mu \rightarrow \nu_e$ and $\nu_\mu \rightarrow \nu_\mu$ SM probabilities at the first order in $a_{\alpha\beta}$ and $c_{\alpha\beta}$ as [41].³

$$P_{\mu e}^{LIV} \sim 2Ls_{13} \sin 2\theta_{23} \sin \Delta \left\{ \mathcal{F}_{e\mu} \left[-c_{23} \sin \Delta \sin(\delta_{CP} + \Phi_{e\mu}) + c_{23} \left(\frac{s_{23}^2 \sin \Delta}{c_{23}^2 \Delta} + \cos \Delta \right) \cos(\delta_{CP} + \Phi_{e\mu}) \right] + \mathcal{F}_{e\tau} \left[s_{23} \sin \Delta \sin(\delta_{CP} + \Phi_{e\tau}) + s_{23} \left(\frac{\sin \Delta}{\Delta} - \cos \Delta \right) \cos(\delta_{CP} + \Phi_{e\tau}) \right] \right\}, \quad (7)$$

where $s_{ij} = \sin \theta_{ij}$, $c_{ij} = \cos \theta_{ij}$, $\Delta = \Delta m_{31}^2 L/4E$ with L is the distance travelled by the neutrino and finally $\mathcal{F}_{\alpha\beta}$ is either $|a_{\alpha\beta}|$ or $-4/3E|c_{\alpha\beta}|$ (the related phases are indicated with $\Phi_{\alpha\beta}$). It is clear that the leading corrections to the standard $P_{\mu e}$ are driven by the $e - \mu$ and $e - \tau$ LIV parameters. For the muon neutrino disappearance, instead, we obtain [41]:

$$P_{\mu\mu}^{LIV} \sim \frac{1}{2} \sin^2 2\theta_{23} \left[2\Delta \sin^2 \theta_{13} - 2L \sin 2\theta_{23} \mathcal{F}_{\mu\tau} \cos \Phi_{\mu\tau} \right]; \quad (8)$$

the main dependence on the LIV parameters is given by $a_{\mu\tau} (c_{\mu\tau})^4$.

Several bounds on the LIV parameter have been obtained using long-baseline accelerator neutrinos [41,42,46–58], short baseline accelerator neutrinos [59,60], reactor neutrinos [61,62], solar neutrinos [63], high-energy astrophysical neutrinos [64–67] and atmospheric neutrinos [68–71] (see also [72,73] for reviews on this, and other, new physics models). Since we are interested in the DUNE experiment performances with a high-energy flux, in the following, we summarize the bounds that DUNE in its standard configuration [23,24,30] might set on off-diagonal LIV parameters. In [41], the authors found, at 95% CL:

$$\begin{aligned} |a_{e\mu}| &< 1.00 \times 10^{-23} \text{ GeV}, & |c_{e\mu}| &< 0.66 \times 10^{-24}, \\ |a_{e\tau}| &< 1.05 \times 10^{-23} \text{ GeV}, & |c_{e\tau}| &< 1.65 \times 10^{-24}, \\ |a_{\mu\tau}| &< 1.26 \times 10^{-23} \text{ GeV}, & |c_{\mu\tau}| &< 0.97 \times 10^{-24}, \end{aligned} \tag{9}$$

which are one order (two orders) of magnitude stronger than the bounds predicted from the current LBL experiments NO ν A and T2K on CPT-violating (CPT-conserving) LIV parameters in Ref. [41]⁵. For $a_{e\mu}$ and $a_{e\tau}$, the authors of [41] observed that there exists a strong correlation among them and the standard θ_{23} and δ_{CP} . This allows for a second minimum in the sensitivity analysis and thus weaker bounds on the parameters; however, given that we fix the atmospheric mixing angle to the lower octant, we will not be able to observe such a behavior. Neglecting this degeneracy, the standard DUNE limits obtained in [41] for $a_{e\mu}$ and $a_{e\tau}$ are stronger than the ones in Equation (9) and are as follows:

$$\begin{aligned} |a_{e\mu}| &< 3.0 \times 10^{-24} \text{ GeV}, \\ |a_{e\tau}| &< 4.5 \times 10^{-24} \text{ GeV}. \end{aligned} \tag{10}$$

3.2. HE-DUNE Results

The HE configuration of the DUNE experiment, as already discussed in Section 2, might allow accelerator neutrino energies from roughly 1 to 15 GeV. In Figure 1, we show the electron appearance (left) and muon disappearance (right) oscillation probabilities with and without LIV. Black lines depict the SM oscillation probabilities computed using the best fits summarized in Table 1 [10,74]. Red lines have been obtained setting CP-odd LIV parameters $a_{e\mu}$, $a_{e\tau}$, $a_{\mu\tau}$ to 2.0×10^{-23} GeV in top, middle and bottom panels, respectively. Orange lines show the effect of $c_{e\mu}$, $c_{e\tau}$, $c_{\mu\tau}$ with a magnitude of 10^{-24} . We also considered two extreme values of the corresponding LIV phase $\Phi_{\alpha\beta}$, namely 0° (dashed lines) and 90° (solid lines). The benchmark values of the LIV parameters have been chosen of the same order of magnitude as the DUNE limits obtained with the standard neutrino flux. The shaded regions correspond to the unoscillated standard (grey) and HE (green) DUNE fluxes in arbitrary units. It is clear that in the appearance case, the most important CPT-odd LIV parameters are $a_{e\mu}$ and $a_{e\tau}$, as clearly visible in Equation (7). From the same equation, one can observe that, at the first oscillation maximum, the correction proportional to $a_{e\mu}$ is positive for both considered values of the LIV phase; on the other hand, it has a plus (minus) sign for $\Phi_{e\tau} = 90^\circ$ ($\Phi_{e\tau} = 0^\circ$) when the $a_{e\tau}$ parameter is taken into account. Regarding CPT-even LIV parameters, their effects on $P_{\mu e}$ become more important for higher neutrino energies, above ~ 4 GeV. Such an energy is located at the high-energy tail of the standard flux and at the peak of the HE flux. For this reason, we expect HE-DUNE to be more sensitive to energy-enhanced CPT-even LIV parameters than DUNE in its standard configuration. We also observe that the most relevant parameter in this case is $c_{e\mu}$.

For the disappearance probability, as already mentioned and explicitly shown in Equation (8), the most important LIV parameters are $a_{\mu\tau}$ and $c_{\mu\tau}$. In Figure 1, we can also observe a slight sensitivity of this channel to the $e - \mu$ parameters, especially in the high-energy region mostly covered by the HE-DUNE.

Table 1. Best-fit value of the neutrino oscillation parameters in the standard three-flavor scenario. The values of the mixing angles and the mass splittings and their 1σ uncertainty intervals are taken from Ref. [10].

Oscillation Parameters (3ν)	Normal Ordering (NO)
θ_{12}°	$33.41^{+0.75}_{-0.72}$
θ_{23}°	$42.2^{+1.1}_{-0.9}$
θ_{13}°	$8.58^{+0.11}_{-0.11}$
δ_{CP}°	232^{+36}_{-26}
Δm_{21}^2 (eV ²)	$7.41^{+0.21}_{-0.20} \times 10^{-5}$
Δm_{31}^2 (eV ²)	$+2.507^{+0.026}_{-0.027} \times 10^{-3}$

We now study the performances of DUNE in its high-energy configuration in constraining the LIV parameters. In order to perform our numerical analysis, we used the GLOBES software v3.2.18 [75,76] and its new physics tool [77]. All the results have been obtained using a Poissonian χ^2 defined as:

$$\chi^2(\vec{\lambda}, a) = \sum_{i=1}^n 2 \left((1+a)T_i - O_i + O_i \log \frac{O_i}{(1+a)T_i} \right) + \frac{a^2}{\sigma_a^2}, \tag{11}$$

where $\vec{\lambda}$ is the set of input oscillation parameters, σ_a is the normalization error, n is the number of energy bins that we fixed to 80 [30], O_i are the observed rates and T_i are the theoretical rates employed in the fit. The systematic uncertainties are included using the *pull method* described in [78,79]. The validity of our analysis has been tested by reproducing the standard DUNE results on standard [30] and non-standard oscillation physics [41,80–82]. Moreover, we checked that the number of events obtained with the DUNE high-energy flux was consistent with the one cited in [16].

In Figure 2, we show the allowed 1, 2, 3 σ contours in the $a_{\alpha\beta} - \Phi_{\alpha\beta}$ (top) and $c_{\alpha\beta} - \Phi_{\alpha\beta}$ planes (bottom). All the analyses have been performed fitting the data obtained using the SM parameters scanning over the LIV parameters one at a time. When computing the $\Delta\chi^2$, defined as:

$$\Delta\chi^2 = \chi^2(a_{\alpha\beta}/c_{\alpha\beta} \neq 0) - \chi^2(a_{\alpha\beta}/c_{\alpha\beta} = 0), \tag{12}$$

we fix all the not-showed LIV parameters to zero and we marginalize in the fit on all the oscillation parameters but the solar ones; we use Gaussian priors with the 1σ uncertainties⁶ as summarized in Table 1 for θ_{23} , θ_{13} and Δm_{31}^2 while leaving δ_{CP} free to vary in all its $[0, 2\pi)^\circ$ range. The red lines in the bottom plots corresponding to $a_{\mu\tau}$ ($c_{\mu\tau}$) depict the effect of the inclusion in the analysis of the ν_τ appearance channel. We have verified that, as expected, in all other LIV parameters, the effect of the ν_τ appearance sample is marginal, a situation very similar to that discussed in [16,18], where a non-negligible impact of the ν_τ events was observed in the $\mu - \tau$ sector only in the context of propagation NSI.

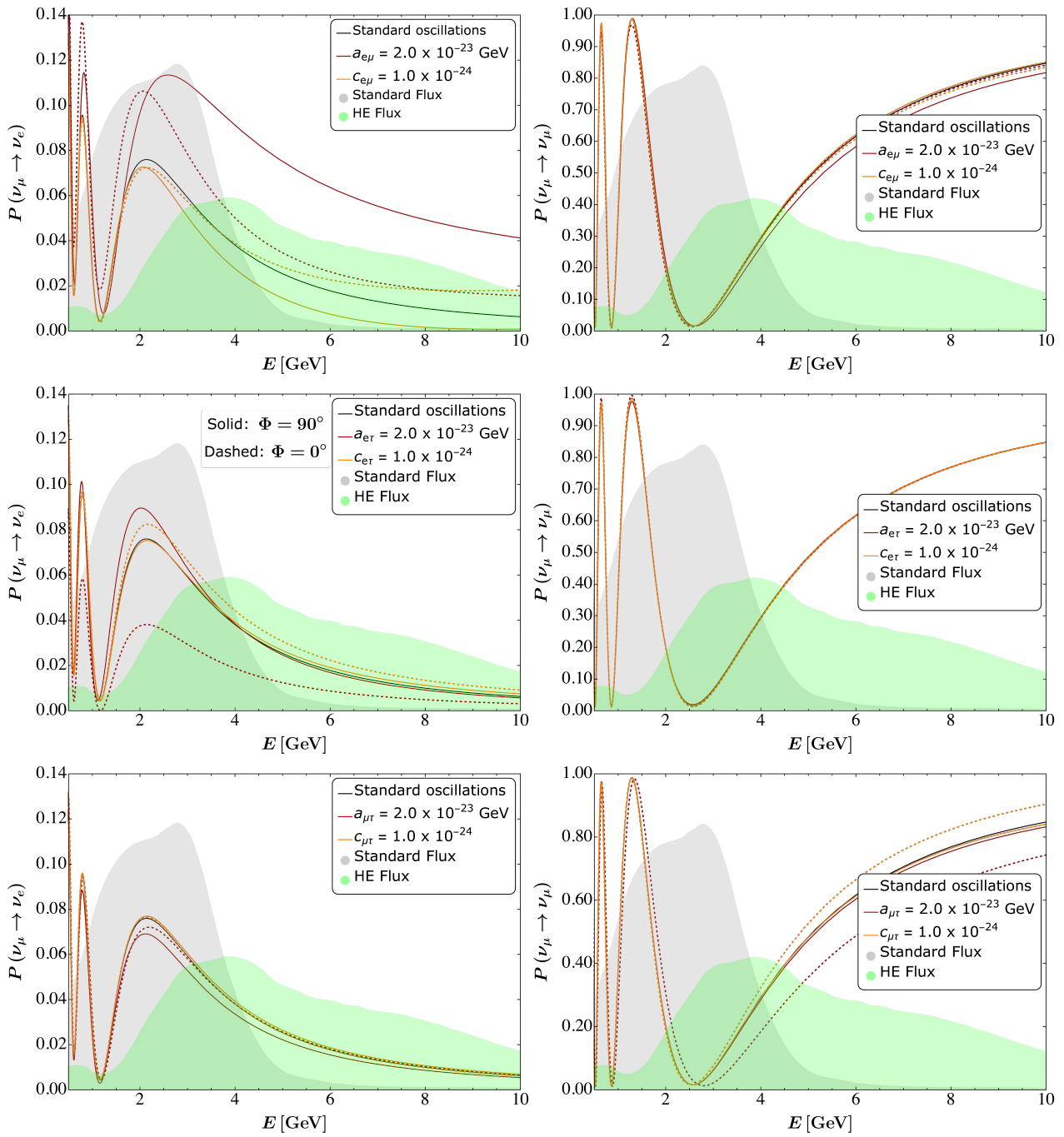


Figure 1. ν_e appearance (left panels) and ν_μ disappearance (right panels) probabilities in the presence of off-diagonal CPT violating and conserving LIV parameters. In particular, the top, middle and bottom panels show the effect of $a_{e\mu}$ ($c_{e\mu}$), $a_{e\tau}$ ($c_{e\tau}$) and $a_{\mu\tau}$ ($c_{\mu\tau}$), respectively. Black lines correspond to the standard oscillation case and red (orange) lines to the probabilities obtained for $a_{\alpha\beta} = 2 \times 10^{-23}$ GeV ($c_{\alpha\beta} = 1.0 \times 10^{-24}$). Solid and dashed curves depict the effects of LIV phases (generally indicated Φ) when $\Phi = 90^\circ$ and $\Phi = 0^\circ$, respectively. The grey and green shadowed regions illustrate the standard and the high-energy DUNE flux.

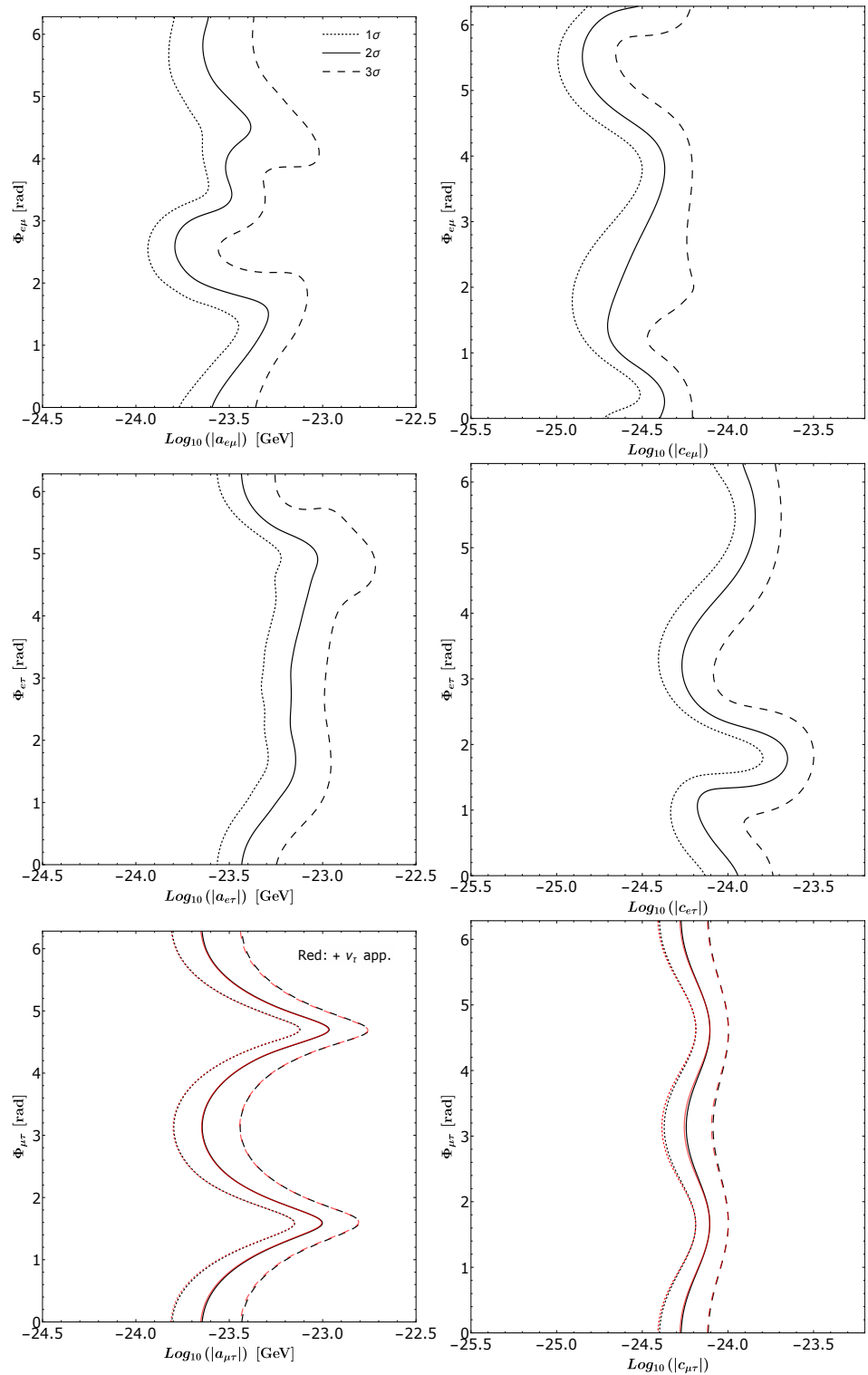


Figure 2. 1σ (dotted), 2σ (solid) and 3σ (dashed) allowed contours in the $|a_{\alpha\beta}| - \Phi_{\alpha\beta}$ (left panels) and $|c_{\alpha\beta}| - \Phi_{\alpha\beta}$ planes (right panels) for HE-DUNE. The red curves in the bottom panels depict the effect of the addition of the ν_τ appearance channel in the analysis.

The 95% limits on the moduli of the LIV parameters, obtained after marginalizing over the corresponding phases, are summarized in Table 2. We observe that by fixing the octant and thus neglecting the degenerate LIV solutions found in [41], the HE-DUNE limits on the $|a_{e\beta}|$ parameters are weaker than the standard DUNE ones. This mainly comes from the fact that the ν_e appearance probability (strongly affected by $|a_{e\beta}|$) and consequently

the number of ν_e events is larger at the first oscillation maximum than at the HE-DUNE energies. On the other hand, the limit on $|a_{\mu\tau}|$ is one order of magnitude more stringent in the HE-DUNE case due to the larger number of ν_μ disappearance events. However, notice that this oscillation channel is strongly affected by the atmospheric mixing angle and by matter effects [83]; thus, the different procedure used in the LIV analysis in Ref. [41], where θ_{23} has been left free to vary in its 3σ allowed range, might have amplified the differences between their standard DUNE and our HE-DUNE results. In fact, we checked that using our same minimization procedure, the standard DUNE bound on $|a_{\mu\tau}|$ would only be worse than the HE-DUNE one by a factor of 2. The interplay between the magnitude of the LIV parameters and their phases is mostly visible in the case of $a_{\mu\tau}$ since the ν_μ disappearance probability is directly proportional to $|a_{\mu\tau}| \cos \Phi_{\mu\tau}$ at the leading order. For this reason, the sensitivity is substantially worse when $\cos \Phi_{\mu\tau} \sim 0$. When considering the other two parameters $a_{e\beta}$, the strong correlations between the new physics phase and the standard phase δ_{CP} make the interpretation of the results as a function of $\Phi_{\alpha\beta}$ less clear. However, it can be seen that the limits on $|a_{e\beta}|$ are only marginally impacted by the value of the LIV phase.

As for the HE-DUNE limits on the CPT-even $c_{\alpha\beta}$ LIV parameters, as expected, they are better than the standard DUNE ones since their effects are amplified by the neutrino energy; the only exception is given by $c_{e\tau}$, which, for $\Phi_{e\tau} \sim 90^\circ$, experiences a worsening in the sensitivity; indeed, as can be seen in Equation (7) and Figure 1, the probabilities when $\Phi_{e\tau} \sim 90^\circ$ are very close to standard ones. Also in this case, except for $c_{\mu\tau}$ (see Equation (8)), the role of the LIV phase on the $|c_{\alpha\beta}|$ limits cannot be easily understood from analytical formulae, but our numerical results show that the limits on $|c_{e\mu}|$ and $|c_{e\tau}|$ do not drastically depend on the new $\Phi_{\alpha\beta}$ phase value.

Table 2. The 95% bounds on the LIV parameters obtained for HE-DUNE. The upper limits have been obtained marginalizing over the LIV phases. The numbers in brackets refer to the foreseen improvement due to the addition of the ν_τ appearance channel in the analysis.

	95% CL limit ($\times 10^{-24}$ GeV)		95% CL limit ($\times 10^{-24}$)
$a_{e\mu}$	<5.1	$c_{e\mu}$	<0.43
$a_{e\tau}$	<9.3	$c_{e\tau}$	<2.23
$a_{\mu\tau}$	<1.12 (<1.0)	$c_{\mu\tau}$	<0.66 (<0.64)

4. The Long-Range Forces Case

As is well known, the neutrino flavor transition can be strongly affected by the presence of a matter medium, which can induce an effective potential modifying the interaction Hamiltonian. However, the presence of BSM interactions between neutrinos and ordinary matter particles can in principle modify the matter potential term in the neutrino Hamiltonian. This is the case, for instance, of the widely studied vector and scalar Non-Standard Interactions (NSIs) [21,84–92]. Another interesting and less studied example is provided by the Long-Range Forces (LRFs) [93–102], which will be described in detail in this section.

4.1. Theoretical Framework

The SM gauge group can be extended by the anomaly-free combination of the $U(1)$ symmetries L_e, L_μ, L_τ and B associated with lepton family number and baryon number. These combinations can be, for instance, $L_e - L_\mu, L_e - L_\tau$ and $L_\mu - L_\tau$ [103–105]⁷. Other combinations have been discussed in the context of neutrino oscillation in [97]. The gauge boson of these symmetries is a massive neutral vector Z' that can mediate new physics interactions between neutrinos and matter. In the case of a large mediator mass, it is possible to study its effect in an Effective Field Theory (EFT) approach, which results in neutrino propagation affected in a vector NSI fashion. If, on the other hand, the mediator is extremely light, the flavor-dependent interaction forces between neutrinos and matter might become important over large distances. Given the huge interaction distance, proportional to $\lambda \sim m_{Z'}^{-1}$,

the matter potential term affecting neutrino oscillation will depend on the matter contained within a radius λ .

Let us first discuss the new interactions arising from these additional symmetries. In addition to the interactions mediated by the SM Z boson, for an $L_\alpha - L_\beta$ symmetry, new Lagrangian terms for the Z' -induced interactions can be written as:

$$\mathcal{L}_{Z'} = g'_{\alpha\beta} Z'_\mu (\bar{l}_\alpha \gamma^\mu l_\alpha - \bar{l}_\beta \gamma^\mu l_\beta + \bar{\nu}_\alpha \gamma^\mu P_L \nu_\alpha - \bar{\nu}_\beta \gamma^\mu P_L \nu_\beta), \tag{13}$$

where ν_α and l_α are the neutrino and the charged lepton fields and P_L is the left-handed projection operator. There also exists a $Z - Z'$ mixed term \mathcal{L}_{mix} that can introduce new four-fermion interactions proportional to the coupling $g'_{\alpha\beta}(\xi - \sin\theta_W\chi)$, where ξ is the rotation angle between the gauge bosons eigenstates, χ is their kinetic mixing angle and θ_W is the usual Weinberg angle [98]. This term allows not only neutrino–lepton new interactions but also new contributions to the neutrino–nucleon scattering. However, since, at large distances, $\mathcal{L}_{Z'} \gg \mathcal{L}_{\text{mix}}$, the mixed term is important only in the $L_\mu - L_\tau$ case, for which neutrino–electron scattering mediated by Z' is prohibited.

All these new interactions involving Z' induce a Yukawa-like potential coming from electrons and neutrons in the Universe which can affect neutrino oscillations [109,110]. For a neutrino at a distance d from a source of a number N_e of electrons and for an $L_e - L_\beta$ symmetry, it can be written as [81,96,98]:

$$V_{e\beta} = G_{e\beta}^2 \frac{N_e}{4\pi d} e^{-m_{Z'} d}. \tag{14}$$

Under the $L_\mu - L_\tau$ symmetry, instead, the LRF effect comes from the mixing between Z' and the SM Z boson. Considering the Universe to be neutral, the net potential, in this case, is only due to a N_n number of neutrons, which generate a potential of the form:

$$V_{\mu\tau} = G_{\mu\tau}^2 \frac{e}{\sin\theta_W \cos\theta_W} \frac{N_n}{4\pi d} e^{-m_{Z'} d}, \tag{15}$$

where e is the electric charge. The effective coupling $G_{\alpha\beta}$ is the equivalent of the coupling $g'_{\alpha\beta}$ in the case of an $L_e - L_\beta$ symmetry while, for the $L_\mu - L_\tau$, it is related to the Lagrangian parameters through the relation $G_{\mu\tau} = \sqrt{g'_{\mu\tau}(\xi - \sin\theta_W\chi)}$.

Let us now consider the effect of LRF on the neutrino oscillations. In general, as previously mentioned, the neutrino propagation Hamiltonian always contains the vacuum and the standard matter potential terms shown in Equation (5). The effect of the potential $V_{\alpha\beta}$ is to add a new contribution of different structures depending on the considered symmetry:

$$H_{LRF} = \begin{pmatrix} V_{e\mu} & 0 & 0 \\ 0 & -V_{e\mu} & 0 \\ 0 & 0 & 0 \end{pmatrix} \text{ for } L_e - L_\mu, \quad H_{LRF} = \begin{pmatrix} V_{e\tau} & 0 & 0 \\ 0 & 0 & 0 \\ 0 & 0 & -V_{e\tau} \end{pmatrix} \text{ for } L_e - L_\tau, \tag{16}$$

$$H_{LRF} = \begin{pmatrix} 0 & 0 & 0 \\ 0 & V_{\mu\tau} & 0 \\ 0 & 0 & -V_{\mu\tau} \end{pmatrix} \text{ for } L_\mu - L_\tau.$$

Notice that the matrices in Equation (16) are similar to the standard matter potential; the main difference between the usual MSW contribution and the LRF one is that the former is a contact potential due to a very massive mediator (the SM Z boson) while the latter encodes the effect of distant electron and neutrons sources on neutrino propagation due to an extremely light mediator (the Z') with a very large interaction length.

The computation of the oscillation probabilities is very cumbersome. In fact, in order to have observable effects of the long-range potentials, we need the quantity $2EV_{\alpha\beta}$ to be comparable to the vacuum oscillation frequency ($\Delta m_{31}^2/2E$ for LBL experiments); this implies that $V_{\alpha\beta} \sim V_{CC} \sim 10^{-14}$ eV, where V_{CC} is the usual matter potential term. Since both

potentials must be included in the evaluation, this produces very lengthy expressions for the transition probabilities. An example of analytical treatment of LRF has been carried out in [96,99,111,112]. Notice that, in principle, LRF probabilities can also be deduced from those computed in the presence of diagonal NSI parameters [96,110,112]. From them, one can recognize that there exists a particular value of the neutrino energy for which a resonance occurs; in the case of $L_e - L_\beta$ symmetries, and neglecting the solar mass difference contribution, this condition reads [99,111]:

$$E_{\text{res}} = \frac{\Delta m_{31}^2 \cos 2\theta_{13}}{2V_{\text{CC}} + 3V_{e\beta}}. \tag{17}$$

This means that the matter resonance occurs in the presence of LRF at lower energies with respect to the standard MSW case. As in the LIV case, LRF has been widely studied in the literature in the context of neutrino oscillation. Limits on the LRF potentials and on the effective coupling appearing in $V_{\alpha\beta}$ were obtained, for example, in [41,81,96,97,100,113–119]. Focusing on the DUNE performances, the Fermilab-based experiment might set the following 95% CL limits on the LRF potentials [81]:

$$\begin{aligned} V_{e\mu} &< 1.9 \times 10^{-14} \text{ eV} \\ V_{e\tau} &< 1.3 \times 10^{-14} \text{ eV} \\ V_{\mu\tau} &< 0.82 \times 10^{-14} \text{ eV}. \end{aligned} \tag{18}$$

The strongest limit can be put on $V_{\mu\tau}$ because it strongly affects the disappearance channel, which has huge statistics in DUNE.

4.2. HE-DUNE Results

In this section, we will explore the capabilities of HE-DUNE to constrain the LRF potential and the limits it might set on the strength of the new forces as well as on the new mediator mass. First, in Figure 3, we plot the effect of long-range potential on the appearance and disappearance probabilities at the DUNE baseline.

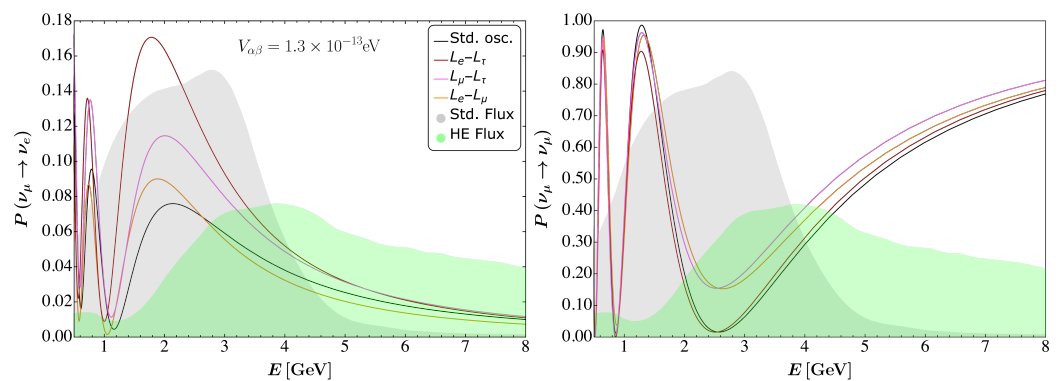


Figure 3. Same as Figure 1, but for the Long-Range Force case. Left (right) plot shows the ν_e appearance (ν_μ disappearance) probability. The red, magenta and orange curves refer to the $L_e - L_\tau$, $L_\mu - L_\tau$ and $L_e - L_\mu$ cases, respectively. The potentials $V_{\alpha\beta}$ have been fixed to 1.3×10^{-13} eV.

The LRF potentials $V_{\alpha\beta}$ have been set to 1.3×10^{-13} eV to show their effects when the LRF is of the same order of magnitude as the standard matter potential. It is clear that the appearance probability is enhanced at the first oscillation maximum for all three cases due to the LRF-potential-induced resonances. In particular, $V_{e\tau}$ has the strongest effect while $V_{e\mu}$ has the mildest one. At higher energies, important for HE-DUNE, we observe that the $V_{\mu\tau}$ decreases the appearance probability while $V_{e\tau}$ and $V_{e\mu}$ increase it. On the other hand, the disappearance probability is enhanced at its first minimum, with $V_{\mu\tau}$ having the

biggest impact for energies above 2.5 GeV. Notice that $V_{e\tau}$ has only a negligible effect on the disappearance probability.

Using the procedure described in Section 3.2, we estimated the bounds that HE-DUNE might be able to set on the LRF potentials. In Figure 4, we show the sensitivity to the three $V_{\alpha\beta}$ as obtained from $\Delta\chi^2$ as:

$$\Delta\chi^2 = \chi^2(V_{\alpha\beta} \neq 0) - \chi^2(V_{\alpha\beta} = 0). \tag{19}$$

We summarize the HE-DUNE 95% CL limits in Table 3. Comparing them with those in Equation (18), we observe that the HE-DUNE could set bounds on $V_{e\beta}$ and $V_{\mu\tau}$ which are 20% and 35% weaker than the DUNE ones, respectively. The reason is that, even though the effect of matter potentials is in general increased for large neutrino energies, long-range potentials cause low-energy resonances in neutrino oscillation probabilities, which can be probed better at the standard DUNE energies.

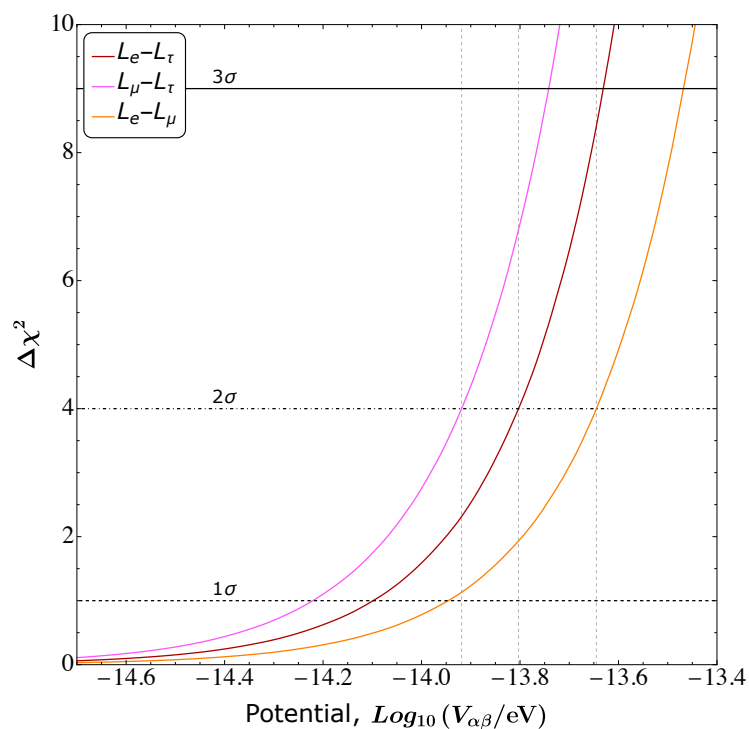


Figure 4. HE-DUNE sensitivity to the LRF potentials. Red, magenta and orange lines correspond to the $L_e - L_\tau$, $L_\mu - L_\tau$ and $L_e - L_\mu$ cases, respectively.

Table 3. The 95% CL limits on the Long-Range Force potentials obtained by HE-DUNE.

	$V_{e\mu}$	$V_{e\tau}$	$V_{\mu\tau}$
95% CL limit	$<2.4 \times 10^{-14}$ eV	$<1.58 \times 10^{-14}$ eV	$<1.23 \times 10^{-14}$ eV

One might use Equations (14) and (15) to find constraints to both the effective Z' coupling and its mass. Following Refs. [81,109], if we want to consider all the matter content of the Universe, we need to take into account neutrinos from matter sources away up to 10^3 Gp, which corresponds to a Z' mediator mass in the range 10^{-10} – 10^{-35} eV. Thus, we are dealing with an effective potential whose most important contributions are:

$$V_{\alpha\beta} = (V_{\alpha\beta})_{\text{Earth}} + (V_{\alpha\beta})_{\text{Moon}} + (V_{\alpha\beta})_{\text{Sun}} + (V_{\alpha\beta})_{\text{Milky Way}} + (V_{\alpha\beta})_{\text{Cosmol}}. \tag{20}$$

In Equation (20), we consider the Moon and the Sun as point-like electron and neutron sources, with $(N_e)_{\text{Moon}} = (N_n)_{\text{Moon}} \sim 5 \times 10^{49}$ and $(N_e)_{\text{Sun}} \sim 4(N_n)_{\text{Sun}} \sim 10^{57}$ [81]. On the

other hand, we modeled the Earth as a continuous distribution with the same average density such as $(N_e)_{\text{Earth}} = (N_n)_{\text{Earth}} \sim 4 \times 10^{51}$; for the Milky Way, we divided the matter content in a thin disk, a thick disk, a central bulge and a diffuse gas, following the reasonings on Refs. [109,120,121], with $(N_e)_{\text{Milky Way}} = (N_n)_{\text{Milky Way}} \sim 10^{67}$. Finally, the cosmological matter has been included in computing the whole potential described in [109] at redshift $z = 0$ as suggested in [81]; the total number of electrons and neutrons in this case has been fixed to $(N_e)_{\text{Cosmol}} \sim 10(N_n)_{\text{Cosmol}} \sim 10^{79}$. Once all the contributions to the long-range potential are estimated, one can constrain both $m_{Z'}$ and $G_{\alpha\beta}$ using the limits on $V_{\alpha\beta}$ in Table 3. Our results are shown in Figure 5 for the three cases $L_e - L_\mu$ (green line), $L_e - L_\tau$ (blue line) and $L_\mu - L_\tau$ (red line). In the upper part of the plot, we show the interaction length $1/m_{Z'}$ corresponding to the given mediator mass. The grey vertical bands show the parameter space excluded by two phenomena [81]: black-hole superradiance and weak gravity conjecture. The former is related to the superradiant growth of an accumulation of very light vector bosons around extremely massive and gravitational bounded objects like supermassive black holes [122]. The latter is related to a lower limit which might be set on the coupling in theories containing both gravity as the weakest force and a $U(1)$ gauge interaction [123].

We can observe that, at the specific distance at which the electron and neutron biggest sources are located, the limits on the effective couplings become stronger. In particular, for mediator masses lower than 10^{-33} eV, which correspond to roughly 10 Gpc (where the causal horizon is located), the bounds on $G_{\alpha\beta}$ become as low as 2.1×10^{-29} for $G_{e\tau}$, 2.6×10^{-29} for $G_{e\mu}$ and 7.5×10^{-29} for $G_{\mu\tau}$. The latter is the weakest limit since it depends on N_n , which is smaller than N_e for cosmological and solar matter, despite corresponding to $V_{\mu\tau}$ which is the potential bounded the most by HE-DUNE.

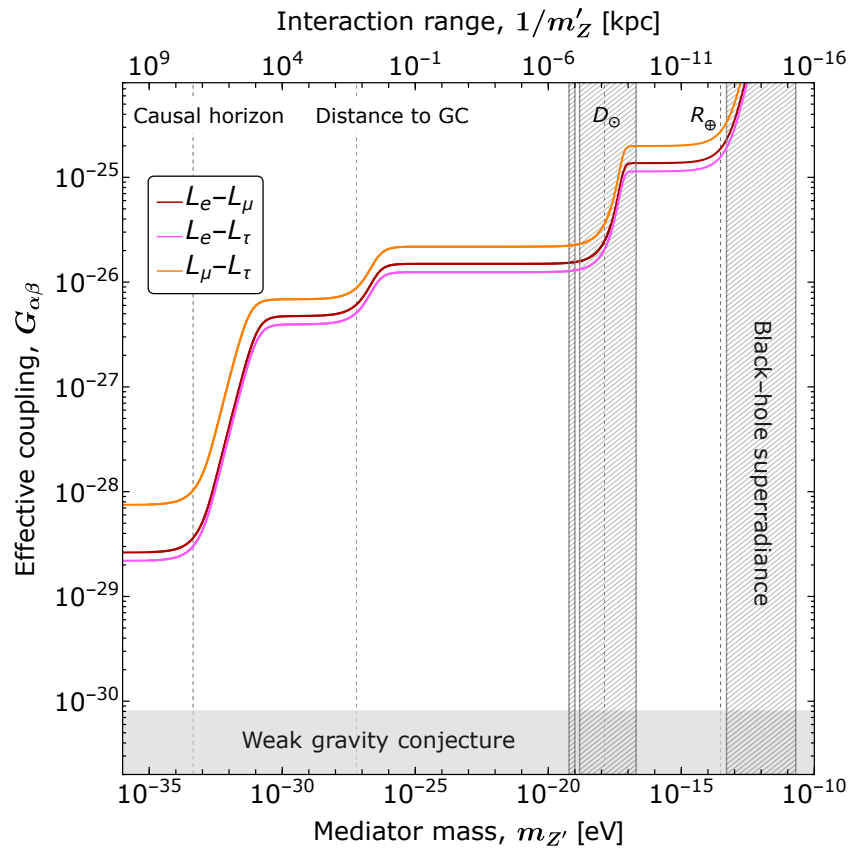


Figure 5. The 95% CL excluded regions in the $m_{Z'} - G_{\alpha\beta}$ plane, fixing the LRF potentials to the 95% CL HE-DUNE limits showed in Table 3. See text for details.

5. The Large Extra Dimensions Case

Neutrino oscillation is not predicted in the original version of the SM since the Higgs mechanism is not capable of providing non-zero neutrino masses and their smallness, compared to the other fermions, is difficult to contemplate in a theoretical general framework. These difficulties can be overcome by several BSM models [124,125]; among them, the Large Extra Dimensions (LEDs) theory [126–133] not only provides a viable framework but also supplies an explanation for the enormous difference between the Electroweak and the Planck scale [134,135]. The main idea is to introduce sterile right-handed neutrino fields, which are singlet under the SM group but propagate in a $4 + N_{ED}$ dimensional space-time, where N_{ED} is the number of space-like extra dimensions. Usual Yukawa Lagrangian terms can then be built using left-handed neutrinos and Higgs fields which live in the usual 4-dimensional space-time. However, the masses coming from such terms are heavily suppressed with respect to other fermion masses due to the much smaller wave function normalizations in the large volume of the extra dimensions. In the following, we will explore the phenomenological implications of the existence of LED on neutrino oscillation.

5.1. Theoretical Framework

Following the approach proposed for neutrino oscillation studies in the context of LED [82,136–146], we will focus on $N_{ED} = 1$; this single LED is compactified on a circle of radius R_{ED} and, for the sterile neutrinos, this gives rise to Kaluza–Klein (KK) modes in the 4-dimensional space-time. It is also possible to consider the presence of more extra dimensions, whose compactification radius is much smaller than R_{ED} without changing the effect of LED on the neutrino oscillation. The model is built by adding three massless five-dimensional fermion fields $\Psi^\alpha = (\psi_L^\alpha, \psi_R^\alpha)$ to the SM. After the compactification of the fifth dimension with the proper boundary conditions, the Ψ^α fields appear in the 4-dimensional space-time as an infinite tower of KK states ψ^n , where n is any integer number. Identifying the zero mode as the right-handed neutrinos $\nu_R^\alpha = \psi_R^{\alpha(0)}$ and writing $\nu_{L,R}^{\alpha(n)} = (\psi_{L,R}^{\alpha(-n)} + \psi_{L,R}^{\alpha(n)})/\sqrt{2}$ [82], the neutrino mass term is [82,127,130,134]:

$$\mathcal{L}_{LED} = m_{\alpha\beta}^D \left(\bar{\nu}_R^\alpha \nu_L^\beta + \sqrt{2} \sum_{n=1}^{\infty} \bar{\nu}_R^{\alpha(n)} \nu_L^\beta \right) + \sum_{n=1}^{\infty} \frac{n}{R_{ED}} \bar{\nu}_R^{\alpha(n)} \nu_L^{\alpha(n)} + h.c., \tag{21}$$

where $m_{\alpha\beta}^D$ is the Dirac mass matrix. Rewriting the mass eigenstates as $N^i = (\nu^{i(0)}, \nu^{i(1)}, \dots)^T$, then \mathcal{L}_{LED} can be written as $\sum_{i=1}^3 \bar{N}_R^i M^i N_L^i$, where the infinite mass matrices is:

$$M_i = \begin{pmatrix} m_i & \sqrt{2}m_i & \sqrt{2}m_i & \dots & \sqrt{2}m_i & \dots \\ 0 & 1/R_{ED} & 0 & \dots & 0 & \dots \\ 0 & 0 & 2/R_{ED} & \dots & 0 & \dots \\ 0 & 0 & 0 & \dots & n/R_{ED} & \dots \\ \vdots & \vdots & \vdots & \vdots & \vdots & \ddots \end{pmatrix}, \tag{22}$$

in which the m_i are the eigenvalues of the neutrino Dirac mass matrix $m_{\alpha\beta}^D$ in Equation (21). The neutrino mixing among the active states is then defined by Equation [82,145]

$$\nu_\alpha = \sum_{i=1}^3 U_{\alpha i} \sum_{n=0}^{\infty} V_{in} \nu_i^{(n)}, \tag{23}$$

where U is the PMNS mixing matrix and V is the *effective mixing matrix* among the KK excitations. Its elements can be written as:

$$(V_{in})^2 = \frac{2}{1 + \pi^2(m_i R_{ED})^2 + (\lambda_i^{(n)})^2 / (m_i R_{ED})^2}, \tag{24}$$

with $\lambda_i^{(n)}$ being the eigenvalues of the matrices $R_{ED}^2 M_i^\dagger M_i$ that can be found as solutions of Equation [82,127,130,137,145]

$$\lambda_i^{(n)} - \pi(m_i R_{ED})^2 \cot(\pi \lambda_i^{(n)}) = 0. \tag{25}$$

Notice that the masses of the KK states are in this case $m_i^{(n)} = \lambda_i^{(n)} / R_{ED}$; since the solutions of Equation (25) satisfy the relation $n \leq \lambda_i^{(n)} < (n + 1/2)$, we can roughly say that $m_i^{(n)} \sim n / R_{ED}$ [82]. Once we fix the experimental observation of the mass splittings to be equal to the differences $\Delta m_{21}^2 = [(\lambda_2^{(0)})^2 - (\lambda_1^{(0)})^2] / R_{ED}^2$ and $\Delta m_{31}^2 = [(\lambda_3^{(0)})^2 - (\lambda_1^{(0)})^2] / R_{ED}^2$, we are left with the standard three neutrinos mixing modified by the effect of the mixing between the active neutrinos and an infinite number of sterile neutrinos. The only non-standard parameters of the model are then the compactification radius R_{ED} and the smallest Dirac mass m_1 . The oscillation probabilities can be obtained, in a vacuum, as

$$P_{\alpha\beta} = \left| \sum_{i=1}^3 \sum_{n=0}^{\infty} U_{\alpha i}^* U_{\beta i} V_{in}^2 \exp\left(-i \frac{(m_i^{(n)})^2 L}{2E}\right) \right| \tag{26}$$

where L is the baseline. In the limit $m_i R_{ED} \rightarrow 0$, we observe that $m_i^{(n)} \rightarrow \infty$ for $n \neq 0$ and $V_{in} \rightarrow \delta_{0n}$, making the oscillation phenomenology identical to the standard one.

It has been shown that, apart from the appearance of new matter resonances at high neutrino energies [136] ($E \gg 1$ TeV), the LED phenomenology does not change significantly if we include more than two KK modes. Indeed, higher modes would imply larger masses $m_i^{(n)}$ and smaller matrix elements V_{in} [145]. Thus, one might study neutrino oscillation in the presence of LED including in the model only a limited number of KK modes. In this context, it is possible to treat the LED case with a number n_{KK} of KK modes as a $3 + 3n_{KK}$ sterile neutrino model [82,136], where all the non-standard mixing angles and mass splittings can be written in terms of the two LED parameters⁸.

The expression of the oscillation probabilities in the LED case is very cumbersome; however, in the limit $m_i R_{ED} \ll 1$, some expansions for the mass eigenstates and mixing matrix elements have been obtained in Refs. [131,145]:

$$\begin{aligned} m_i^{(0)} &= m_i \left[1 - \frac{\pi^2}{6} (m_i R_{ED})^2 + \dots \right] \sim m_i \\ m_i^{(n)} &= \frac{n}{R_{ED}} \left[1 + \frac{(m_i R_{ED})^2}{n^2} + \dots \right] \sim \frac{n}{R_{ED}} \\ V_{i0} &= 1 - \frac{\pi^2}{6} (m_i R_{ED})^2 + \dots \sim 1 \\ V_{in} &= \sqrt{2} \frac{m_i R_{ED}}{n} \left[1 - \frac{3}{2} \frac{(m_i R_{ED})^2}{n^2} + \dots \right] \sim \sqrt{2} \frac{m_i R_{ED}}{n} \end{aligned} \tag{27}$$

from which it is clear that, as already mentioned, the corrections to the standard oscillation case become negligible as n increases.

The complete picture of neutrino oscillation in the presence of LED is obtained when matter effects are added. Then, the oscillation probabilities can be obtained by solving the Schroedinger-like evolution Equation [82]

$$i \frac{d}{dr} N_i = \frac{1}{2E} M_i^\dagger M_i N_i + \sum_{j=1}^3 \lim_{n \rightarrow \infty} \begin{pmatrix} \rho_{ij} & 0_{1 \times n} \\ 0_{n \times 1} & 0_{n \times n} \end{pmatrix} N_j, \tag{28}$$

where the N_i infinite vector of neutrino states and M_i matrices have already been defined in Equation (22) and above, while the quantity ρ_{ij} is defined as

$$\rho_{ij} = \sum_{\alpha} U_{\alpha i}^* U_{\alpha j} (\delta_{\alpha e} V_{CC} - V_{NC}), \tag{29}$$

with U being the standard 3×3 PMNS matrix, $V_{CC} = \sqrt{2}G_F n_e$ the usual matter potential and $V_{NC} = -2\sqrt{2}G_F n_n$ the neutral current matter potential that can no longer be neglected due to the presence of sterile states.

The limits that current experiments could set on the parameter space in the LED case have been discussed, for instance, in Ref. [145]. Notice also that the short baseline, reactor and gallium anomalies, which have been explained with the presence of light sterile neutrinos, could be explained in the presence of LEDs [82,142,145]. In the context of the future DUNE experiment, the expected performances of the experiment have been explored in detail in Ref. [82]. The upper limits on the R_{ED} parameter depend on the lightest neutrino mass value; in particular, in the scenario when $m_1 \rightarrow 0$ eV and the probabilities only depend on R_{ED} , we expect for DUNE at 95% CL:

$$R_{ED} < 0.32 \text{ } \mu\text{m}, \tag{30}$$

while for $m_1 \sim 0.05$ eV, we expect

$$R_{ED} < 0.22 \text{ } \mu\text{m}. \tag{31}$$

On the other hand, it is impossible to set an absolute limit on m_1 unless data are generated considering $R_{ED} \neq 0$; in that case, DUNE might set a lower limit on the absolute neutrino mass [82]⁹.

5.2. HE-DUNE Results

In this section, we discuss the effects of LED at HE-DUNE. For the ν_e appearance and ν_μ disappearance probabilities (see Figure 6), we consider as a reference two possible lightest neutrino masses m_1 , namely 0.0 and 0.05 eV. For the compactification radius, we choose $0.5 \text{ } \mu\text{m}$, which corresponds to $R_{ED}^{-1} = 0.38 \text{ eV}^{-1}$. In our computations, we included three KK modes, even though we checked that our results were only negligibly affected by the inclusion of the second and third KK modes. From Figure 6, we see that the main effect of LED is the occurrence of new fast oscillations driven by the large mass splittings between the active states and the heavy KK excitations. The amplitude of the oscillations depends on the values of the V_{in} matrix elements. In addition, the presence of LED decreases both the appearance and disappearance probabilities at the first oscillation maximum since the value of V_{i0} is always less than 1; see Equation (27). Moreover, at a fixed R_{ED} , the probabilities in general decrease as m_1 increases. The differences between probabilities around the first oscillation maximum (DUNE) and the high-energy region (HE-DUNE) are mainly due to the fact that fast oscillation driven by KK becomes slower and with a larger amplitude when the neutrino energy increases. For this reason, with high-energy neutrinos, it might be possible to resolve these oscillations allowing for better constraints on the LED model [73].

In Figure 7, we show the allowed parameters space in the $R_{ED} - m_1$ plane in the HE-DUNE case. The analysis has been performed using the procedure described in the previous two sections. Here, we can see that at 2σ the weakest limit for R_{ED} reached for $m_1 \rightarrow 0$ is $0.258 \text{ } \mu\text{m}$. This constraint is better than the standard DUNE one. As noted above, one of the main reasons for that is the possibility of recognizing fast oscillations at higher energies, where they occur with a smaller frequency with respect to the lower energy region probed by standard DUNE. Another interesting feature is that for $m_1 < 0.04$ eV, the HE-DUNE constraint on R_{ED} becomes independent of the lightest neutrino mass. This means that if m_1 is, for instance, 0.05 eV, then the standard DUNE experiment outperforms HE-DUNE (see Equation (31)).

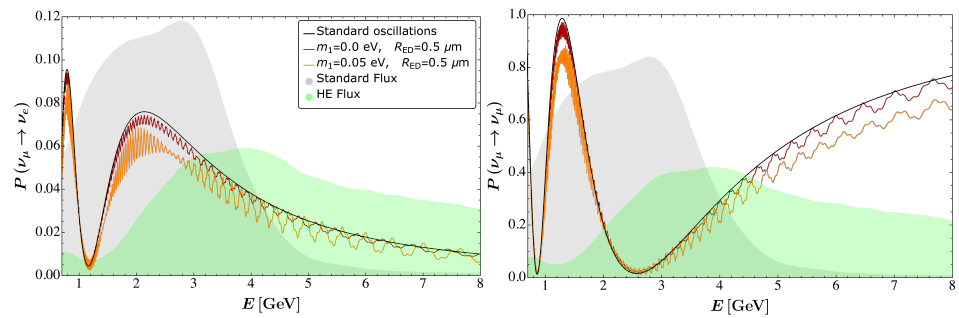


Figure 6. Same as Figure 1 but in the Large Extra Dimension case. Red (orange) curves have been obtained fixing $R_{ED} = 0.5 \mu\text{m}$ and $m_1 = 0.0 \text{ eV}$ ($m_1 = 0.05 \text{ eV}$).

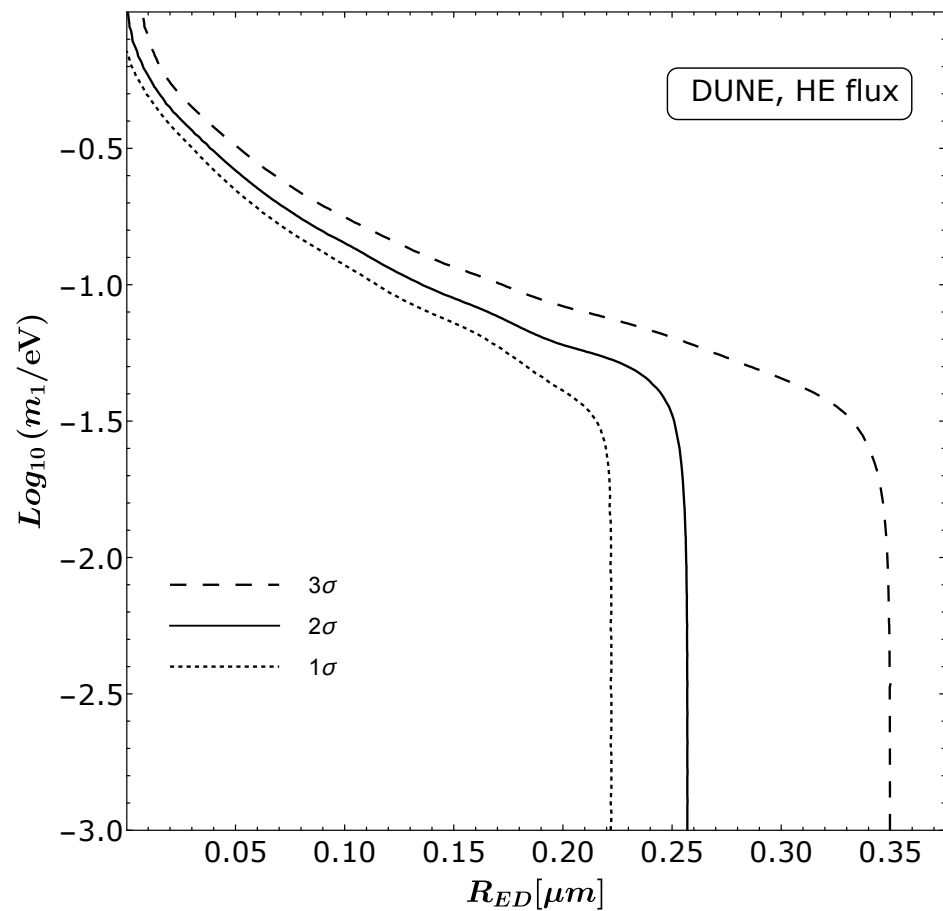


Figure 7. 1σ (dotted) 2σ (solid) and 3σ (dashed) allowed regions in the $R_{ED} - m_1$ plane for HE-DUNE.

6. Conclusions

Neutrino oscillation is the best-established phenomenon beyond the Standard Model of particle physics. Despite several experiments that have been able to measure the oscillation parameters with a few percent uncertainty, there are still some unknowns like the neutrino mass hierarchy and the amount of leptonic CP violation (if any). Moreover, oscillation searches are of great interest since several new physics models can affect neutrino propagation and thus modify the related probabilities. Future oscillation facilities are expected to reach great precision in the measurements of the mixing parameters; at the same time, they could provide a great probe for new physics models involving neutrinos. In this work, we considered the capabilities of the high-energy flux configuration of the future DUNE experiment (HE-DUNE). The possibility of employing this broad neutrino flux, which might reach more than 15 GeV in energy, has been envisaged in order to have access

to $\nu_\mu \rightarrow \nu_\tau$ oscillations, which could not be easily observed with the standard DUNE configuration due to the energy threshold of CC ν_τ interactions. In addition, HE-DUNE could in principle also be very useful to constrain new physics scenarios where the non-standard oscillation effects are more pronounced at high energies. Among them, Non-Standard Interactions, sterile neutrinos, non-unitarity of the PMNS matrix and quantum decoherence have already been studied in the literature [16–21].

In this work, we considered three different new physics models:

- **Lorentz Invariance Violation (LIV):** in this model, the neutrino Lagrangian density is modified through several Lorentz-violating operators, both CPT-even and CPT-odd. The presence of such operators modifies the neutrino propagation Hamiltonian with the addition of two Hermitian matrices $a_{\alpha\beta}$ (CPT-violating) and $c_{\alpha\beta}$ (CPT-conserving). The effects of the second matrix increase linearly with the neutrino energy. We studied in Section 3.2 the sensitivity of HE-DUNE to the off-diagonal LIV parameters. We found that the limits on the moduli of CPT-violating parameters $|a_{\alpha\beta}|$ are worse than the ones that the standard DUNE is expected to set. On the other hand, HE-DUNE capabilities should exceed the standard DUNE ones in constraining energy-enhanced effects of CPT-conserving LIV parameters $|c_{\alpha\beta}|$.
- **Long-Range Forces (LRFs):** in this model, we expect that new interactions with an ultra-light mediator, with a very long interaction length, arise from a gauge $U(1)$ symmetry of the form $L_\alpha - L_\beta$. These interactions can modify the matter potential term in the neutrino oscillation Hamiltonian. We showed that the limits from HE-DUNE on this new potential are rather stringent but not enough to overcome the standard DUNE ones. We also computed the limits on the coupling of the new interaction as well as on the mass of the new mediator. These are correlated with the interaction length since, depending on that, neutrinos might experience the potential generated from various astrophysical matter densities.
- **Large Extra Dimensions (LEDs):** if right-handed neutrinos are singlets under the SM group, but they can propagate in space-time with more than four dimensions, the smallness of neutrino masses can be naturally explained. In the case in which one of the new dimensions is compactified in a sphere with a relatively large radius, the Kaluza–Klein excitations of the neutrino states can be treated as sterile neutrinos involved in the oscillation. In this approach, the transition probabilities depend not only on the standard mixing parameters but also on the smallest Dirac neutrino mass and on the compactification radius R_{ED} of the large extra dimension. We showed that the limit that HE-DUNE might set on R_{ED} , for small enough lightest neutrino mass, is better than the standard DUNE one. This is because the fast active–sterile oscillations coming from the Kaluza–Klein states might be resolved better at high energies than at lower ones.

In conclusion, the DUNE high-energy flux might be useful not only to collect a large sample of ν_τ events but also to set stringent limits on new physics parameters. This suggests that an HE-DUNE run could provide much information on the BSM neutrino physics, which are complementary to the standard DUNE ones.

Author Contributions: Conceptualization: A.G., S.M. and D.M.; Methodology: A.G., S.M. and D.M.; Formal analysis: A.G., S.M. and D.M.; Writing: A.G., S.M. and D.M. All authors have read and agreed to the published version of the manuscript.

Funding: This research received no external funding.

Data Availability Statement: Data are contained within the article.

Conflicts of Interest: The authors declare no conflicts of interest.

Notes

- ¹ For the other two oscillation channels, namely ν_e appearance and ν_μ disappearance, the collaboration suggested 2% and 5%, respectively.
- ² In Quantum Field Theory the *CPT theorem* states that the combination of the discrete transformations “Chargeconjugation” (C), “Parity” (P) and “Timereversal” (T) must be a symmetry of the theory.
- ³ The LIV probabilities shown here have been obtained in [41] neglecting also terms proportional to α^2 and $\alpha \sin \theta_{13}$ where $\alpha = \Delta m_{21}^2 / \Delta m_{31}^2$.
- ⁴ The ν_τ appearance probability can be obtained from unitarity and the leading term will be the one depending again on $a_{\mu\tau}$ ($c_{\mu\tau}$).
- ⁵ Notice that limits from the more energetic atmospheric and astrophysical neutrinos on CPT-even LIV parameters are more stringent than the DUNE ones due to the dependence on the neutrino energy of their effect on the oscillation probabilities.
- ⁶ In our analysis, we assume that the octant of θ_{23} is known; in particular, as suggested by global fits in [10,74], to lie in the lower octant.
- ⁷ In [106–108], it has been shown that $L_\alpha - L_\beta$ gauge symmetries can predict viable neutrino masses and mixing with the addition of Higgs-like particles charged under the new symmetries.
- ⁸ Notice that a general model with sterile neutrinos cannot be mimicked by a LED model in general; for instance, the presence of Large Extra Dimensions does not generate new sources of CP violation, unlike the sterile neutrinos hypothesis [21,82].
- ⁹ In [73,146], DUNE analyses have been repeated using a different experimental configuration; they found weaker limits on R_{ED} .

References

1. Fukuda, Y.; Hayakawa, T.; Ichihara, E.; Inoue, K.; Ishihara, K.; Ishino, H.; Itow, Y.; Kajita, T.; 554 Kameda, J.; Kasuga, S.; et al. Evidence for oscillation of atmospheric neutrinos. *Phys. Rev. Lett.* **1998**, *81*, 1562–1567. [[CrossRef](#)]
2. Xu, X.J.; Wang, Z.; Chen, S. Solar neutrino physics. *Prog. Part. Nucl. Phys.* **2023**, *131*, 104043. [[CrossRef](#)]
3. Choubey, S. Atmospheric neutrinos: Status and prospects. *Nucl. Phys. B* **2016**, *908*, 235–249. [[CrossRef](#)]
4. Wen, L.J.; Cao, J.; Wang, Y.F. Reactor Neutrino Experiments: Present and Future. *Ann. Rev. Nucl. Part. Sci.* **2017**, *67*, 183–211. [[CrossRef](#)]
5. Mezzetto, M.; Terranova, F. Three-flavour oscillations with accelerator neutrino beams. *Universe* **2020**, *6*, 32. [[CrossRef](#)]
6. Gando, A.; Gando, Y.; Ichimura, K.; Ikeda, H.; Inoue, K.; Kibe, Y.; Kishimoto, Y.; Koga, M.; Minekawa, Y.; Mitsui, T.; et al. Precision Measurement of Neutrino Oscillation Parameters with KamLAND. *Phys. Rev. Lett.* **2008**, *100*, 221803. [[CrossRef](#)]
7. Gando, A.; Gando, Y.; Ichimura, K.; Ikeda, H.; Inoue, K.; Kibe, Y.; Kishimoto, Y.; Koga, M.; Minekawa, Y.; Mitsui, T.; et al. Constraints on θ_{13} from A Three-Flavor Oscillation Analysis of Reactor Antineutrinos at KamLAND. *Phys. Rev. D* **2011**, *83*, 052002. [[CrossRef](#)]
8. Gando, A.; Gando, Y.; Hanakago, H.; Ikeda, H.; Inoue, K.; Ishidoshiro, K.; Ishikawa, H.; Koga, M.; Matsuda, R.; Matsuda, S.; et al. Reactor On-Off Antineutrino Measurement with KamLAND. *Phys. Rev. D* **2013**, *88*, 033001. [[CrossRef](#)]
9. An, F.P.; Bai, J.Z.; Balantekin, A.B.; Band, H.R.; Beavis, D.; Beriguete, W.; Bishai, M.; Blyth, S.; Boddy, K.; Brown, R.L.; et al. Observation of electron-antineutrino disappearance at Daya Bay. *Phys. Rev. Lett.* **2012**, *108*, 171803. [[CrossRef](#)]
10. Esteban, I.; Gonzalez-Garcia, M.C.; Maltoni, M.; Schwetz, T.; Zhou, A. The fate of hints: Updated global analysis of three-flavor neutrino oscillations. *J. High Energy Phys.* **2020**, *9*, 178. [[CrossRef](#)]
11. Abe, K.; Abe, K.; Aihara, H.; Aimi, A.; Akutsu, R.; Andreopoulos, C.; Anghel, I.; Anthony, L.H.V.; Antonova, M.; Ashida, Y.; et al. Hyper-Kamiokande Design Report. *arXiv* **2018**, arXiv:1805.04163.
12. Acciarri, R.; Acero, M.A.; Adamowski, M.; Adams, C.; Adamson, P.; Adhikari, S.; Ahmad, Z.; Albright, C.H.; Alion, T.; Amador, E.; et al. Long-Baseline Neutrino Facility (LBNF) and Deep Underground Neutrino Experiment (DUNE): Conceptual Design Report, Volume 2: The Physics Program for DUNE at LBNF. *arXiv* **2015**, arXiv:1512.06148.
13. Himmel, A. New Oscillation Results from the NOvA Experiment. 2020. Available online: <https://www.osti.gov/biblio/1640225/> (accessed on 15 March 2024).
14. Batkiewicz-Kwasniak, M. The Latest T2K Neutrino Oscillation Results and the Future of the T2K and Hyper-Kamiokande Experiments. *Acta Phys. Polon. Supp.* **2022**, *15*, 23. [[CrossRef](#)]
15. Rahaman, U.; Raut, S. On the tension between the latest NOvA and T2K data. *arXiv* **2021**, arXiv:2112.13186.
16. Ghoshal, A.; Giarnetti, A.; Meloni, D. On the role of the ν_τ appearance in DUNE in constraining standard neutrino physics and beyond. *J. High Energy Phys.* **2019**, *12*, 126. [[CrossRef](#)]
17. Masud, M.; Bishai, M.; Mehta, P. Extricating New Physics Scenarios at DUNE with Higher Energy Beams. *Sci. Rep.* **2019**, *9*, 352. [[CrossRef](#)]
18. De Gouvêa, A.; Kelly, K.J.; Stenico, G.V.; Pasquini, P. Physics with Beam Tau-Neutrino Appearance at DUNE. *Phys. Rev. D* **2019**, *100*, 016004. [[CrossRef](#)]
19. De Romeri, V.; Giunti, C.; Stuttard, T.; Ternes, C.A. Neutrino oscillation bounds on quantum decoherence. *J. High Energy Phys.* **2023**, *9*, 97. [[CrossRef](#)]
20. Mammen Abraham, R.; Alvarez-Muñiz, J.; Argüelles, C.A.; Ariga, A.; Ariga, T.; Aurisano, A.; Autiero, D.; Bishai, M.; Bostan, N.; Bustamante, M.; et al. Tau neutrinos in the next decade: From GeV to EeV. *J. Phys. G* **2022**, *49*, 110501. [[CrossRef](#)]

21. Giarnetti, A.; Meloni, D. New Sources of Leptonic CP Violation at the DUNE Neutrino Experiment. *Universe* **2021**, *7*, 240. [[CrossRef](#)]
22. Acciarri, R.; Acero, M.A.; Adamowski, M.; Adams, C.; Adamson, P.; Adhikari, S.; Ahmad, Z.; Albright, C.H.; Alion, T.; Amador, E.; et al. Long-Baseline Neutrino Facility (LBNF) and Deep Underground Neutrino Experiment (DUNE): Conceptual Design Report, Volume 1: The LBNF and DUNE Projects. *arXiv* **2016**, arXiv:1601.05471.
23. Abi, B.; Acciarri, R.; Acero, M.A.; Adamov, G.; Adams, D.; Adinolfi, M.; Ahmad, Z.; Ahmed, J.; Alion, T.; Monsalve, S.A.; et al. Long-baseline neutrino oscillation physics potential of the DUNE experiment. *Eur. Phys. J. C* **2020**, *80*, 978. [[CrossRef](#)]
24. Abi, B.; Acciarri, R.; Acero, M.A.; Adamov, G.; Adams, D.; Adinolfi, M.; Ahmad, Z.; Ahmed, J.; Alion, T.; Monsalve, S.A.; et al. Deep Underground Neutrino Experiment (DUNE), Far Detector Technical Design Report, Volume II: DUNE Physics. *arXiv* **2020**, arXiv:2002.03005.
25. Abud, A.A.; Abi, B.; Acciarri, R.; Acero, M.A.; Adamov, G.; Adams, D.; Adinolfi, M.; Aduszkiewicz, A.; Ahmad, Z.; Ahmed, J.; et al. Deep Underground Neutrino Experiment (DUNE) Near Detector Conceptual Design Report. *Instruments* **2021**, *5*, 31. [[CrossRef](#)]
26. Fermilab. Available online: <http://home.fnal.gov/~ljf26/DUNEFluxes/> (accessed on 15 March 2024).
27. Bishai, M.; Dolce, M. Optimization of the LBNF/DUNE Beamline for Tau Neutrinos. Available online: http://docs.dunescience.org/cgi-bin/RetrieveFile?docid=2013&filename=DOLCE_M_report.pdf&version=1 (accessed on 15 March 2024).
28. DUNE Neutrino Flux Files Generated with G4LBNF. Available online: <https://glaucus.crc.nd.edu/DUNEFluxes/> (accessed on 15 March 2024).
29. Alion, T.; Back, J.J.; Bashyal, A.; Bass, M.; Bishai, M.; Cherdack, D.; Diwan, M.; Djurcic, Z.; Evans, J.; Fernandez-Martinez, E.; et al. Experiment Simulation Configurations Used in DUNE CDR. *arXiv* **2016**, arXiv:1606.09550.
30. Abi, B.; Acciarri, R.; Acero, M.A.; Adamov, G.; Adams, D.; Adinolfi, M.; Ahmad, Z.; Ahmed, J.; Alion, T.; Monsalve, S.A.; et al. Experiment Simulation Configurations Approximating DUNE TDR. *arXiv* **2021**, arXiv:2103.04797.
31. Colladay, D.; Kostelecky, V.A. CPT violation and the standard model. *Phys. Rev. D* **1997**, *55*, 6760–6774. [[CrossRef](#)]
32. Colladay, D.; Kostelecky, V.A. Lorentz violating extension of the standard model. *Phys. Rev. D* **1998**, *58*, 116002. [[CrossRef](#)]
33. Diaz, J.S.; Kostelecky, A. Lorentz- and CPT-violating models for neutrino oscillations. *Phys. Rev. D* **2012**, *85*, 016013. [[CrossRef](#)]
34. Greenberg, O.W. CPT violation implies violation of Lorentz invariance. *Phys. Rev. Lett.* **2002**, *89*, 231602. [[CrossRef](#)]
35. Kostelecky, V.A.; Potting, R. CPT and strings. *Nucl. Phys. B* **1991**, *359*, 545–570. [[CrossRef](#)]
36. Kostelecky, V.A.; Potting, R. CPT, strings, and meson factories. *Phys. Rev. D* **1995**, *51*, 3923–3935. [[CrossRef](#)]
37. Kostelecky, V.A.; Potting, R. Expectation values, Lorentz invariance, and CPT in the open bosonic string. *Phys. Lett. B* **1996**, *381*, 89–96 [[CrossRef](#)]
38. Kostelecky, V.A.; Mewes, M. Lorentz and CPT violation in neutrinos. *Phys. Rev. D* **2004**, *69*, 016005. [[CrossRef](#)]
39. Kostelecký, V.A.; Samuel, S. Spontaneous breaking of Lorentz symmetry in string theory. *Phys. Rev. D* **1989**, *39*, 683–685. [[CrossRef](#)] [[PubMed](#)]
40. Kostelecký, V.A.; Samuel, S. Phenomenological gravitational constraints on strings and higher-dimensional theories. *Phys. Rev. Lett.* **1989**, *63*, 224–227. [[CrossRef](#)]
41. Agarwalla, S.K.; Das, S.; Sahoo, S.; Swain, P. Constraining Lorentz invariance violation with next-generation long-baseline experiments. *J. High Energy Phys.* **2023**, *7*, 216. [[CrossRef](#)]
42. Kumar Agarwalla, S.; Masud, M. Can Lorentz invariance violation affect the sensitivity of deep underground neutrino experiment? *Eur. Phys. J. C* **2020**, *80*, 716. [[CrossRef](#)]
43. Kostelecky, A.; Mewes, M. Neutrinos with Lorentz-violating operators of arbitrary dimension. *Phys. Rev. D* **2012**, *85*, 096005. [[CrossRef](#)]
44. Wolfenstein, L. Neutrino oscillations in matter. *Phys. Rev. D* **1978**, *17*, 2369–2374. [[CrossRef](#)]
45. Barenboim, G.; Ternes, C.A.; Tórtola, M. New physics vs. new paradigms: Distinguishing CPT violation from NSI. *Eur. Phys. J. C* **2019**, *79*, 390. [[CrossRef](#)]
46. Diaz, J.S. Correspondence between nonstandard interactions and CPT violation in neutrino oscillations. *arXiv* **2015**, arXiv:1506.01936.
47. Barenboim, G.; Masud, M.; Ternes, C.A.; Tórtola, M. Exploring the intrinsic Lorentz-violating parameters at DUNE. *Phys. Lett. B* **2019**, *788*, 308–315. [[CrossRef](#)]
48. Fiza, N.; Khan Chowdhury, N.R.; Masud, M. Investigating Lorentz Invariance Violation with the long baseline experiment P2O. *J. High Energy Phys.* **2023**, *1*, 76. [[CrossRef](#)]
49. Adamson, P.; Andreopoulos, C.; Arms, K.E.; Armstrong, R.; Auty, D.J.; Ayres, D.S.; Baller, B.; Barr, G.; Barrett, W.L.; Becker, B.R.; et al. Testing Lorentz Invariance and CPT Conservation with NuMI Neutrinos in the MINOS Near Detector. *Phys. Rev. Lett.* **2008**, *101*, 151601. [[CrossRef](#)]
50. Adamson, P.; Andreopoulos, C.; Arms, K.E.; Armstrong, R.; Auty, D.J.; Ayres, D.S.; Baller, B.; Barr, G.; Barrett, W.L.; Becker, B.R.; et al. A Search for Lorentz Invariance and CPT Violation with the MINOS Far Detector. *Phys. Rev. Lett.* **2010**, *105*, 151601. [[CrossRef](#)] [[PubMed](#)]
51. Adamson, P.; Andreopoulos, C.; Arms, K.E.; Armstrong, R.; Auty, D.J.; Ayres, D.S.; Baller, B.; Barr, G.; Barrett, W.L.; Becker, B.R.; et al. Search for Lorentz invariance and CPT violation with muon antineutrinos in the MINOS Near Detector. *Phys. Rev. D* **2012**, *85*, 031101. [[CrossRef](#)]

52. Dighe, A.; Ray, S. CPT violation in long baseline neutrino experiments: A Three flavor analysis. *Phys. Rev. D* **2008**, *78*, 036002. [[CrossRef](#)]
53. Barenboim, G.; Lykken, J.D. MINOS and CPT-violating neutrinos. *Phys. Rev. D* **2009**, *80*, 113008. [[CrossRef](#)]
54. Rebel, B.; Mufson, S. The Search for Neutrino-Antineutrino Mixing Resulting from Lorentz Invariance Violation using Neutrino Interactions in MINOS. *Astropart. Phys.* **2013**, *48*, 78–81. [[CrossRef](#)]
55. de Gouvêa, A.; Kelly, K.J. Neutrino vs. Antineutrino Oscillation Parameters at DUNE and Hyper-Kamiokande. *Phys. Rev. D* **2017**, *96*, 095018. [[CrossRef](#)]
56. Barenboim, G.; Ternes, C.A.; Tórtola, M. Neutrinos, DUNE and the world best bound on CPT invariance. *Phys. Lett. B* **2018**, *780*, 631–637. [[CrossRef](#)]
57. Majhi, R.; Chembra, S.; Mohanta, R. Exploring the effect of Lorentz invariance violation with the currently running long-baseline experiments. *Eur. Phys. J. C* **2020**, *80*, 364. [[CrossRef](#)]
58. Majhi, R.; Singha, D.K.; Ghosh, M.; Mohanta, R. Distinguishing nonstandard interaction and Lorentz invariance violation at the Protvino to super-ORCA experiment. *Phys. Rev. D* **2023**, *107*, 075036. [[CrossRef](#)]
59. Abe, K.; Amey, J.; Andreopoulos, C.; Antonova, M.; Aoki, S.; Ariga, A.; Assylbekov, S.; Autiero, D.; Ban, S.; Barbato, F.C.T.; et al. Search for Lorentz and CPT violation using sidereal time dependence of neutrino flavor transitions over a short baseline. *Phys. Rev. D* **2017**, *95*, 111101. [[CrossRef](#)]
60. Aguilar-Arevalo, A.A.; Anderson, C.E.; Bazarko, A.O.; Brice, S.J.; Brown, B.C.; Bugel, L.; Cao, J.; Coney, L.; Conrad, J.M.; Cox, D.C.; et al. Test of Lorentz and CPT violation with Short Baseline Neutrino Oscillation Excesses. *Phys. Lett. B* **2013**, *718*, 1303–1308. [[CrossRef](#)]
61. Giunti, C.; Laveder, M. Hint of CPT Violation in Short-Baseline Electron Neutrino Disappearance. *Phys. Rev. D* **2010**, *82*, 113009. [[CrossRef](#)]
62. Abe, Y.; Aberle, C.; dos Anjos, J.C.; Bergevin, M.; Bernstein, A.; Bezerra, T.J.C.; Bezrukhov, L.; Blucher, E.; Bowden, N.S.; Buck, C.; et al. First Test of Lorentz Violation with a Reactor-based Antineutrino Experiment. *Phys. Rev. D* **2012**, *86*, 112009. [[CrossRef](#)]
63. Diaz, J.S.; Schwetz, T. Limits on CPT violation from solar neutrinos. *Phys. Rev. D* **2016**, *93*, 093004. [[CrossRef](#)]
64. Hooper, D.; Morgan, D.; Winstanley, E. Lorentz and CPT invariance violation in high-energy neutrinos. *Phys. Rev. D* **2005**, *72*, 065009. [[CrossRef](#)]
65. Tomar, G.; Mohanty, S.; Pakvasa, S. Lorentz Invariance Violation and IceCube Neutrino Events. *J. High Energy Phys.* **2015**, *11*, 22. [[CrossRef](#)]
66. Liao, J.; Marfatia, D. IceCube’s astrophysical neutrino energy spectrum from CPT violation. *Phys. Rev. D* **2018**, *97*, 041302. [[CrossRef](#)]
67. Abbasi, R.; Abdou, Y.; Abu-Zayyad, T.; Adams, J.; Aguilar, J.A.; Ahlers, M.; Andeen, K.; Auffenberg, J.; Bai, X.; Baker, M.; et al. Search for a Lorentz-violating sidereal signal with atmospheric neutrinos in IceCube. *Phys. Rev. D* **2010**, *82*, 112003. [[CrossRef](#)]
68. Chatterjee, A.; Gandhi, R.; Singh, J. Probing Lorentz and CPT Violation in a Magnetized Iron Detector using Atmospheric Neutrinos. *J. High Energy Phys.* **2014**, *6*, 45. [[CrossRef](#)]
69. Sahoo, S.; Kumar, A.; Agarwalla, S.K. Probing Lorentz Invariance Violation with atmospheric neutrinos at INO-ICAL. *J. High Energy Phys.* **2022**, *3*, 50. [[CrossRef](#)]
70. Datta, A.; Gandhi, R.; Mehta, P.; Sankar, S.U. Atmospheric neutrinos as a probe of CPT and Lorentz violation. *Phys. Lett. B* **2004**, *597*, 356–361. [[CrossRef](#)]
71. Abe, K.; Haga, Y.; Hayato, Y.; Ikeda, M.; Iyogi, K.; Kameda, J.; Kishimoto, Y.; Miura, M.; Moriyama, S.; Nakahata, M.; et al. Test of Lorentz invariance with atmospheric neutrinos. *Phys. Rev. D* **2015**, *91*, 052003. [[CrossRef](#)]
72. Argüelles, C.A.; Aurisano, A.J.; Batell, B.; Berger, J.; Bishai, M.; Boschi, T.; Byrnes, N.; Chatterjee, A.; Chodos, A.; Coan, T.; et al. New opportunities at the next-generation neutrino experiments I: BSM neutrino physics and dark matter. *Rept. Prog. Phys.* **2020**, *83*, 124201. [[CrossRef](#)]
73. Argüelles, C.A.; Barenboim, G.; Bustamante, M.; Coloma, P.; Denton, P.B.; Esteban, I.; Farzan, Y.; Martínez, E.F.; Forero, D.V.; Gago, A.M.; et al. Snowmass white paper: Beyond the standard model effects on neutrino flavor: Submitted to the proceedings of the US community study on the future of particle physics (Snowmass 2021). *Eur. Phys. J. C* **2023**, *83*, 15. [[CrossRef](#)]
74. NuFit 5.2. 2022. Available online: www.nu-fit.org (accessed on 15 March 2024).
75. Huber, P.; Lindner, M.; Winter, W. Simulation of long-baseline neutrino oscillation experiments with GLOBES (General Long Baseline Experiment Simulator). *Comput. Phys. Commun.* **2005**, *167*, 195. [[CrossRef](#)]
76. Huber, P.; Kopp, J.; Lindner, M.; Rolinec, M.; Winter, W. New features in the simulation of neutrino oscillation experiments with GLOBES 3.0: General Long Baseline Experiment Simulator. *Comput. Phys. Commun.* **2007**, *177*, 432–438. [[CrossRef](#)]
77. Kopp, J.; Lindner, M.; Ota, T.; Sato, J. Non-standard neutrino interactions in reactor and superbeam experiments. *Phys. Rev. D* **2008**, *77*, 013007. [[CrossRef](#)]
78. Huber, P.; Lindner, M.; Winter, W. Superbeams versus neutrino factories. *Nucl. Phys. B* **2002**, *645*, 3–48. [[CrossRef](#)]
79. Fogli, G.L.; Lisi, E.; Marrone, A.; Montanino, D.; Palazzo, A. Getting the most from the statistical analysis of solar neutrino oscillations. *Phys. Rev. D* **2002**, *66*, 053010. [[CrossRef](#)]
80. Abi, B.; Acciarri, R.; Acero, M.A.; Adamov, G.; Adams, D.; Adinolfi, M.; Ahmad, Z.; Ahmed, J.; Alion, T.; Monsalve, S.A.; et al. Prospects for beyond the Standard Model physics searches at the Deep Underground Neutrino Experiment. *Eur. Phys. J. C* **2021**, *81*, 322. [[CrossRef](#)]

81. Singh, M.; Bustamante, M.; Agarwalla, S.K. Flavor-dependent long-range neutrino interactions in DUNE & T2HK: Alone they constrain, together they discover. *J. High Energy Phys.* **2023**, *8*, 101. [[CrossRef](#)]
82. Berryman, J.M.; de Gouvêa, A.; Kelly, K.J.; Peres, O.L.G.; Tabrizi, Z. Large, Extra Dimensions at the Deep Underground Neutrino Experiment. *Phys. Rev. D* **2016**, *94*, 033006. [[CrossRef](#)]
83. Agarwalla, S.K.; Das, S.; Giarnetti, A.; Meloni, D.; Singh, M. Enhancing sensitivity to leptonic CP violation using complementarity among DUNE, T2HK, and T2HKK. *Eur. Phys. J. C* **2023**, *83*, 694. [[CrossRef](#)]
84. Denton, P.B.; Gehrlein, J.; Pestes, R. CP-Violating Neutrino Nonstandard Interactions in Long-Baseline-Accelerator Data. *Phys. Rev. Lett.* **2021**, *126*, 051801. [[CrossRef](#)]
85. de Gouvêa, A.; Kelly, K.J. Non-standard Neutrino Interactions at DUNE. *Nucl. Phys. B* **2016**, *908*, 318–335. [[CrossRef](#)]
86. Neutrino Non-Standard Interactions: A Status Report. *SciPost Phys. Proc.* **2019**, *2*, 1. [[CrossRef](#)]
87. Bakhti, P.; Rajaei, M. Sensitivities of future reactor and long-baseline neutrino experiments to NSI. *Phys. Rev. D* **2021**, *103*, 075003. [[CrossRef](#)]
88. Ge, S.F.; Parke, S.J. Scalar Nonstandard Interactions in Neutrino Oscillation. *Phys. Rev. Lett.* **2019**, *122*, 211801. [[CrossRef](#)] [[PubMed](#)]
89. Denton, P.B.; Giarnetti, A.; Meloni, D. How to identify different new neutrino oscillation physics scenarios at DUNE. *J. High Energy Phys.* **2023**, *2*, 210. [[CrossRef](#)]
90. Aguilar, J.; Anastasopoulos, M.; Baussan, E.; Bhattacharyya, A.K.; Bignami, A.; Blennow, M.; Bogomilov, M.; Bolling, B.; Bouquerel, E.; Bramati, F.; et al. Study of non-standard interaction mediated by a scalar field at ESSnuSB experiment. *arXiv* **2023**, arXiv:2310.10749.
91. Gupta, A.; Majumdar, D.; Prakash, S. Neutrino oscillation measurements with JUNO in the presence of scalar NSI. *arXiv* **2023**, arXiv:2306.07343.
92. Sarker, A.; Medhi, A.; Bezboruah, D.; Devi, M.M.; Dutta, D. Impact of scalar NSI on the neutrino mass hierarchy sensitivity at DUNE, T2HK and T2HKK. *arXiv* **2023**, arXiv:2309.12249.
93. Grifols, J.A.; Masso, E.; Peris, S. Supernova neutrinos as probes of long range nongravitational interactions of dark matter. *Astropart. Phys.* **1994**, *2*, 161–165. [[CrossRef](#)]
94. Grifols, J.A.; Masso, E.; Toldra, R. Majorana neutrinos and long range forces. *Phys. Lett. B* **1996**, *389*, 563–565. [[CrossRef](#)]
95. Grifols, J.A.; Masso, E. Neutrino oscillations in the sun probe long range leptonic forces. *Phys. Lett. B* **2004**, *579*, 123–126. [[CrossRef](#)]
96. Mishra, P.; Majhi, R.; Pusty, S.K.; Ghosh, M.; Mohanta, R. Study of Long Range Force in P2SO and T2HKK. *arXiv* **2024**, arXiv:2402.19178.
97. Agarwalla, S.K.; Bustamante, M.; Singh, M.; Swain, P. A plethora of long-range neutrino interactions probed by DUNE and T2HK. *arXiv* **2024**, arXiv:2404.02775.
98. Agarwalla, S.K.; Bustamante, M.; Das, S.; Narang, A. Present and future constraints on flavor-dependent long-range interactions of high-energy astrophysical neutrinos. *J. High Energy Phys.* **2023**, *8*, 113. [[CrossRef](#)]
99. Chatterjee, S.S.; Dasgupta, A.; Agarwalla, S.K. Exploring Flavor-Dependent Long-Range Forces in Long-Baseline Neutrino Oscillation Experiments. *J. High Energy Phys.* **2015**, *12*, 167. [[CrossRef](#)]
100. Coloma, P.; Gonzalez-Garcia, M.C.; Maltoni, M. Neutrino oscillation constraints on $U(1)'$ models: From non-standard interactions to long-range forces. *J. High Energy Phys.* **2021**, *1*, 114; Erratum in: *J. High Energy Phys.* **2022**, *11*, 115. . [[CrossRef](#)]
101. Smirnov, A.Y.; Xu, X.J. Wolfenstein potentials for neutrinos induced by ultra-light mediators. *J. High Energy Phys.* **2019**, *12*, 46. [[CrossRef](#)]
102. Chauhan, G.; Xu, X.J. Impact of the cosmic neutrino background on long-range force searches. *J. High Energy Phys.* **2024**, *7*, 255. [[CrossRef](#)]
103. He, X.G.; Joshi, G.C.; Lew, H.; Volkas, R.R. New- Z' phenomenology. *Phys. Rev. D* **1991**, *43*, R22–R24. [[CrossRef](#)]
104. He, X.G.; Joshi, G.C.; Lew, H.; Volkas, R.R. Simplest Z' model. *Phys. Rev. D* **1991**, *44*, 2118–2132. [[CrossRef](#)]
105. Foot, R.; He, X.G.; Lew, H.; Volkas, R.R. Model for a light Z' -prime boson. *Phys. Rev. D* **1994**, *50*, 4571–4580. [[CrossRef](#)]
106. Asai, K.; Hamaguchi, K.; Nagata, N.; Tseng, S.Y.; Tsumura, K. Minimal Gauged $U(1)_{L_\alpha-L_\beta}$ Models Driven into a Corner. *Phys. Rev. D* **2019**, *99*, 055029. [[CrossRef](#)]
107. Asai, K.; Hamaguchi, K.; Nagata, N. Predictions for the neutrino parameters in the minimal gauged $U(1)_{L_\mu-L_\tau}$ model. *Eur. Phys. J. C* **2017**, *77*, 763. [[CrossRef](#)]
108. Lou, Y.; Nomura, T. Neutrino observables in gauged $U(1)_{L_\alpha-L_\beta}$ models with two Higgs doublet and one singlet scalars. *arXiv* **2024**, arXiv:2406.01030.
109. Bustamante, M.; Agarwalla, S.K. Universe's Worth of Electrons to Probe Long-Range Interactions of High-Energy Astrophysical Neutrinos. *Phys. Rev. Lett.* **2019**, *122*, 061103. [[CrossRef](#)] [[PubMed](#)]
110. Wise, M.B.; Zhang, Y. Lepton Flavorful Fifth Force and Depth-dependent Neutrino Matter Interactions. *J. High Energy Phys.* **2018**, *6*, 53. [[CrossRef](#)]
111. Khatun, A.; Thakore, T.; Kumar Agarwalla, S. Can INO be Sensitive to Flavor-Dependent Long-Range Forces? *J. High Energy Phys.* **2018**, *4*, 23. [[CrossRef](#)]
112. Agarwalla, S.K.; Das, S.; Masud, M.; Swain, P. Evolution of neutrino mass-mixing parameters in matter with non-standard interactions. *J. High Energy Phys.* **2021**, *11*, 94. [[CrossRef](#)]

113. Joshipura, A.S.; Mohanty, S. Constraints on flavor dependent long range forces from atmospheric neutrino observations at super-Kamiokande. *Phys. Lett. B* **2004**, *584*, 103–108. [[CrossRef](#)]
114. Bandyopadhyay, A.; Dighe, A.; Joshipura, A.S. Constraints on flavor-dependent long range forces from solar neutrinos and KamLAND. *Phys. Rev. D* **2007**, *75*, 093005. [[CrossRef](#)]
115. Gonzalez-Garcia, M.C.; Maltoni, M. Determination of matter potential from global analysis of neutrino oscillation data. *J. High Energy Phys.* **2013**, *9*, 152. [[CrossRef](#)]
116. Honda, M.; Kao, Y.; Okamura, N.; Pronin, A.; Takeuchi, T. Constraints on New Physics from Long Baseline Neutrino Oscillation Experiments. *arXiv* **2007**, arXiv:0707.4545.
117. Farzan, Y.; Palomares-Ruiz, S. Flavor of cosmic neutrinos preserved by ultralight dark matter. *Phys. Rev. D* **2019**, *99*, 051702. [[CrossRef](#)]
118. Aartsen, M.G.; Abbasi, R.; Ackermann, M.; Adams, J.; Aguilar, J.A.; Ahlers, M.; Ahrens, M.; Alispach, C.; Allison, P.; Amin, N.M.; et al. IceCube-Gen2: The window to the extreme Universe. *J. Phys. G* **2021**, *48*, 060501. [[CrossRef](#)]
119. Heeck, J.; Rodejohann, W. Gauged $L_\mu - L_\tau$ and different Muon Neutrino and Anti-Neutrino Oscillations: MINOS and beyond. *J. Phys. G* **2011**, *38*, 085005. [[CrossRef](#)]
120. McMillan, P.J. Mass models of the Milky Way. *Mon. Not. R. Astron. Soc.* **2011**, *414*, 2446–2457. [[CrossRef](#)]
121. Miller, M.J.; Bregman, J.N. The Structure of the Milky Way's Hot Gas Halo. *Astrophys. J.* **2013**, *770*, 118. [[CrossRef](#)]
122. Baryakhtar, M.; Lasenby, R.; Teo, M. Black Hole Superradiance Signatures of Ultralight Vectors. *Phys. Rev. D* **2017**, *96*, 035019. [[CrossRef](#)]
123. Arkani-Hamed, N.; Motl, L.; Nicolis, A.; Vafa, C. The String landscape, black holes and gravity as the weakest force. *J. High Energy Phys.* **2007**, *6*, 60. [[CrossRef](#)]
124. de Gouvêa, A. Neutrino Mass Models. *Ann. Rev. Nucl. Part. Sci.* **2016**, *66*, 197–217. [[CrossRef](#)]
125. King, S.F. Neutrino mass models. *Rept. Prog. Phys.* **2004**, *67*, 107–158. [[CrossRef](#)]
126. Arkani-Hamed, N.; Dimopoulos, S.; Dvali, G.R.; March-Russell, J. Neutrino masses from large extra dimensions. *Phys. Rev. D* **2001**, *65*, 024032. [[CrossRef](#)]
127. Dienes, K.R.; Dudas, E.; Gherghetta, T. Neutrino oscillations without neutrino masses or heavy mass scales: A Higher dimensional seesaw mechanism. *Nucl. Phys. B* **1999**, *557*, 25. [[CrossRef](#)]
128. Dvali, G.R.; Smirnov, A.Y. Probing large extra dimensions with neutrinos. *Nucl. Phys. B* **1999**, *563*, 63–81. [[CrossRef](#)]
129. Mohapatra, R.N.; Perez-Lorenzana, A. Three flavor neutrino oscillations in models with large extra dimensions. *Nucl. Phys. B* **2001**, *593*, 451–470. [[CrossRef](#)]
130. Barbieri, R.; Creminelli, P.; Strumia, A. Neutrino oscillations from large extra dimensions. *Nucl. Phys. B* **2000**, *585*, 28–44. [[CrossRef](#)]
131. Davoudiasl, H.; Langacker, P.; Perelstein, M. Constraints on large extra dimensions from neutrino oscillation experiments. *Phys. Rev. D* **2002**, *65*, 105015. [[CrossRef](#)]
132. Antoniadis, I.; Arkani-Hamed, N.; Dimopoulos, S.; Dvali, G.R. New dimensions at a millimeter to a Fermi and superstrings at a TeV. *Phys. Lett. B* **1998**, *436*, 257–263. [[CrossRef](#)]
133. Antoniadis, I.; Kiritsis, E.; Rizos, J.; Tomaras, T.N. D-branes and the standard model. *Nucl. Phys. B* **2003**, *660*, 81–115. [[CrossRef](#)]
134. Arkani-Hamed, N.; Dimopoulos, S.; Dvali, G.R. The Hierarchy problem and new dimensions at a millimeter. *Phys. Lett. B* **1998**, *429*, 263–272. [[CrossRef](#)]
135. Arkani-Hamed, N.; Dimopoulos, S.; Dvali, G.R. Phenomenology, astrophysics and cosmology of theories with submillimeter dimensions and TeV scale quantum gravity. *Phys. Rev. D* **1999**, *59*, 086004. [[CrossRef](#)]
136. Esmaili, A.; Peres, O.L.G.; Tabrizi, Z. Probing Large Extra Dimensions with IceCube. *J. Cosmol. Astropart. Phys.* **2014**, *12*, 2. [[CrossRef](#)]
137. Machado, P.A.N.; Nunokawa, H.; Zukanovich Funchal, R. Testing for Large Extra Dimensions with Neutrino Oscillations. *Phys. Rev. D* **2011**, *84*, 013003. [[CrossRef](#)]
138. Machado, P.A.N.; Nunokawa, H.; dos Santos, F.A.P.; Funchal, R.Z. Bulk Neutrinos as an Alternative Cause of the Gallium and Reactor Anti-neutrino Anomalies. *Phys. Rev. D* **2012**, *85*, 073012. [[CrossRef](#)]
139. Basto-Gonzalez, V.S.; Esmaili, A.; Peres, O.L.G. Kinematical Test of Large Extra Dimension in Beta Decay Experiments. *Phys. Lett. B* **2013**, *718*, 1020–1023. [[CrossRef](#)]
140. Girardi, I.; Meloni, D. Constraining new physics scenarios in neutrino oscillations from Daya Bay data. *Phys. Rev. D* **2014**, *90*, 073011. [[CrossRef](#)]
141. Rodejohann, W.; Zhang, H. Signatures of Extra Dimensional Sterile Neutrinos. *Phys. Lett. B* **2014**, *737*, 81–89. [[CrossRef](#)]
142. Carena, M.; Li, Y.Y.; Machado, C.S.; Machado, P.A.N.; Wagner, C.E.M. Neutrinos in Large Extra Dimensions and Short-Baseline ν_e Appearance. *Phys. Rev. D* **2017**, *96*, 095014. [[CrossRef](#)]
143. Stenico, G.V.; Forero, D.V.; Peres, O.L.G. A Short Travel for Neutrinos in Large Extra Dimensions. *J. High Energy Phys.* **2018**, *11*, 155. [[CrossRef](#)]
144. Basto-Gonzalez, V.S.; Forero, D.V.; Giunti, C.; Quiroga, A.A.; Ternes, C.A. Short-baseline oscillation scenarios at JUNO and TAO. *Phys. Rev. D* **2022**, *105*, 075023. [[CrossRef](#)]

-
145. Forero, D.V.; Giunti, C.; Ternes, C.A.; Tyagi, O. Large extra dimensions and neutrino experiments. *Phys. Rev. D* **2022**, *106*, 035027. [[CrossRef](#)]
 146. Roy, S. Capability of the proposed long-baseline experiments to probe large extra dimension. *Phys. Rev. D* **2023**, *108*, 055015. [[CrossRef](#)]

Disclaimer/Publisher's Note: The statements, opinions and data contained in all publications are solely those of the individual author(s) and contributor(s) and not of MDPI and/or the editor(s). MDPI and/or the editor(s) disclaim responsibility for any injury to people or property resulting from any ideas, methods, instructions or products referred to in the content.